ANTON DE KOM UNIVERSITY OF SURINAME
FACULTY OF TECHNOLOGY
DEPARTMENT OF GEOLOGY AND MINING

Statistical analysis of geochemical data and petrogenesis of the gabbroic-ultramafic bodies in Suriname

A thesis submitted in the partial fulfillment of the requirements for the degree of

Master of Science in Mineral Geosciences

by

Sonja S. Oedai

June 2019

APPROVAL FOR FINAL THESIS

To: Prof. Dr. Th. E. Wong,

Coordinator of the Master in Mineral Geosciences

The thesis written by Sonja Oedai, entitled "***Statistical analysis of geochemical data and petrogenesis of the gabbroic-ultramafic bodies in Suriname***" has been approved in respect to style and intellectual content and is referred to you for judgment.

We have read this thesis and recommended that it be approved.

…….

Prof. Dr. S.B. Kroonenberg

(Endowed Professor of Dep. Geology and Mining)

Supervisor

Date of defense:

The thesis of Sonja Oedai is approved.

……

Prof. Dr. Th. E. Wong

(Coordinator of the MSc. in Mineral Geosciences)

Head of the Department Geology and Mining

Abstract

This research describes the statistical analysis of geochemical data and petrogenesis of the gabbroic-ultramafic bodies in Suriname. Recent investigation show that there are two different generations of gabbroic-ultramafic bodies in the Shield: the Lucie gabbro (western region, 2147 Ma) and the Bemau ultramafitite (the eastern region, 1985 Ma). The processing of the geochemical data (INAA and XRF) is done by SPSS. The petrological interpretations with the computer program GCDkit and Past3. The geochemistry shows for both regions that the rock are divided in subalkaline/Tholeiitic basic rocks, ultramafic and gabbro-norite. The analysis shows a distinction between the two suites. These differences can be explained as follows: 1). West intruded in granitoid rocks, and had incorporated more Si, K and Na. The eastern suite intruded mostly in mafic Paramaka rocks in the greenstone belt, and therefore has been less contaminated with Si, K and Na, and had higher Mg, Ni and Cr. 2). Possible incomplete data set in the east, because of limited number of samples and possible sampling bias. The gabbroic-ultramafic bodies in the Guiana Shield of Suriname resembles the ultramafic complexes in Alaska and the Urals. These originates from a depleted mantle source that has undergone metasomatism in a subduction setting. Furthermore tholeiitic rocks are produced by volcanism in the oceans at mid-ocean-ridges. The magma is from the earth's mantle because of the occurrences of olivine and pyroxene. Both eastern and western bodies present characteristics of Alaskan type intrusions

Acknowledgements

Foremost, I would like to express my sincere gratitude to Prof. Dr. S. B. Kroonenberg for the continuous support of my master research, for his patience, motivation, most of all inspiration and of course the immense knowledge. His guidance helped me in all the time of research and writing of this thesis. I could not have imagined having a better mentor for this research.

I would like to thank Prof. Dr. Th.Wong for encouraging me to do my research on this topic, Ms. Nicole Kioe-A-Sen, Msc. who was always ready to help me throughout my entire course.

I very much appreciated the willingness from Prof. Dr. P, M. Kroonenberg to help us with the analysis using SPSS.

Finally I would like to express my gratitude to my family and colleagues from Natin-MBO for their encouragement through the final process of the writing.

Table of contents

List of figures

List of tables

1. Introduction

In the years 1978-1981 the geologists, Bosma, W., Maas, K. and Roever de, E.W.F. conducted a geochemical project (WOTRO: 75-197) to study the petrogenesis and the geochemical characteristics of the gabbroic-ultramafic intrusive bodies in Suriname, De Goeje Gabbros. The data were manually analyzed and interpreted, but were never published.

For this thesis, the available data on 87 rock samples are processed and interpreted with the computer program, GCDkit, Past3 and statistically analysed using SPSS.

The next paragraphs describe a historical review and the hypothesis for the study.

1.1. A historical review related to the research

The Paleoproterozoic basement of Suriname consists of the Marowijne Greenstone Belt in the northeastern part of the country, including adjacent older granites, the high-grade metamorphic Bakhuis Granulite Belt and Coeroeni Gneiss Belt in northwestern and southwestern Suriname, respectively, and a huge granitoid-felsic volcanic terrain in the central and southern part of the country (fig. 1.1.). The basement originated largely during the Trans-Amazonian Orogeny, 2.26-2.05 Ga (Bosma. et al., 1983).

This research describes gabbroic-ultramafic rocks in the basement which form part of a geological unit that was formerly known as De Goeje Gabbro. They occur as small intrusive bodies, scattered within both the metamorphic belts and the granitoid-volcanic terrains. This type of gabbroic rocks was thought to be genetically related to the Trans-Amazonian granitoid magmatism of the Guiana Shield (de Vletter De, 1984; Bosma, et al. 1983).

On the 1:500000 Geological Map of Suriname of 1977 the distribution of over 200 gabbroic and/or ultramafic bodies classified with the De Goeje Gabbro has been indicated. Apart from the De Goeje Gabbro this map also distinguishes metamorphosed gabbroic rocks forming part of the metamorphosed volcanic-sedimentary greenstone belt complex in the NE. Recent investigation, however, show that there are two different generations of gabbroic-ultramafic bodies in the Shield: the Lucie gabbro and the Bemau ultramafitite. The first one is associated with the greenstone belt and adjacent older granites in eastern Suriname, the Bemau and De Goeje complexes, dated in French Guiana at around 2147 Ma (Delor et al.., 2003a in Kroonenberg et al.., 2016). The second one is a much younger suite in western and central Suriname, the Lucie Gabbro, dated at 1985 Ma.

Gabbroic rocks are considered a possible source rock of platinum minerals, and alluvial platinum has been found in the De Goeje mountains. Also, gabbroic bodies elsewhere in Suriname might represent potential platinum bearers (Bosma, et al. 1980 (unpublished)). With this in mind, the present project was started to evaluate the vast amount of unpublished geochemical data, to allow an adequate interpretation of the origin of the gabbroic-ultramafic rocks of De Goeje-type and to understand the relation between the two suites of different ages.

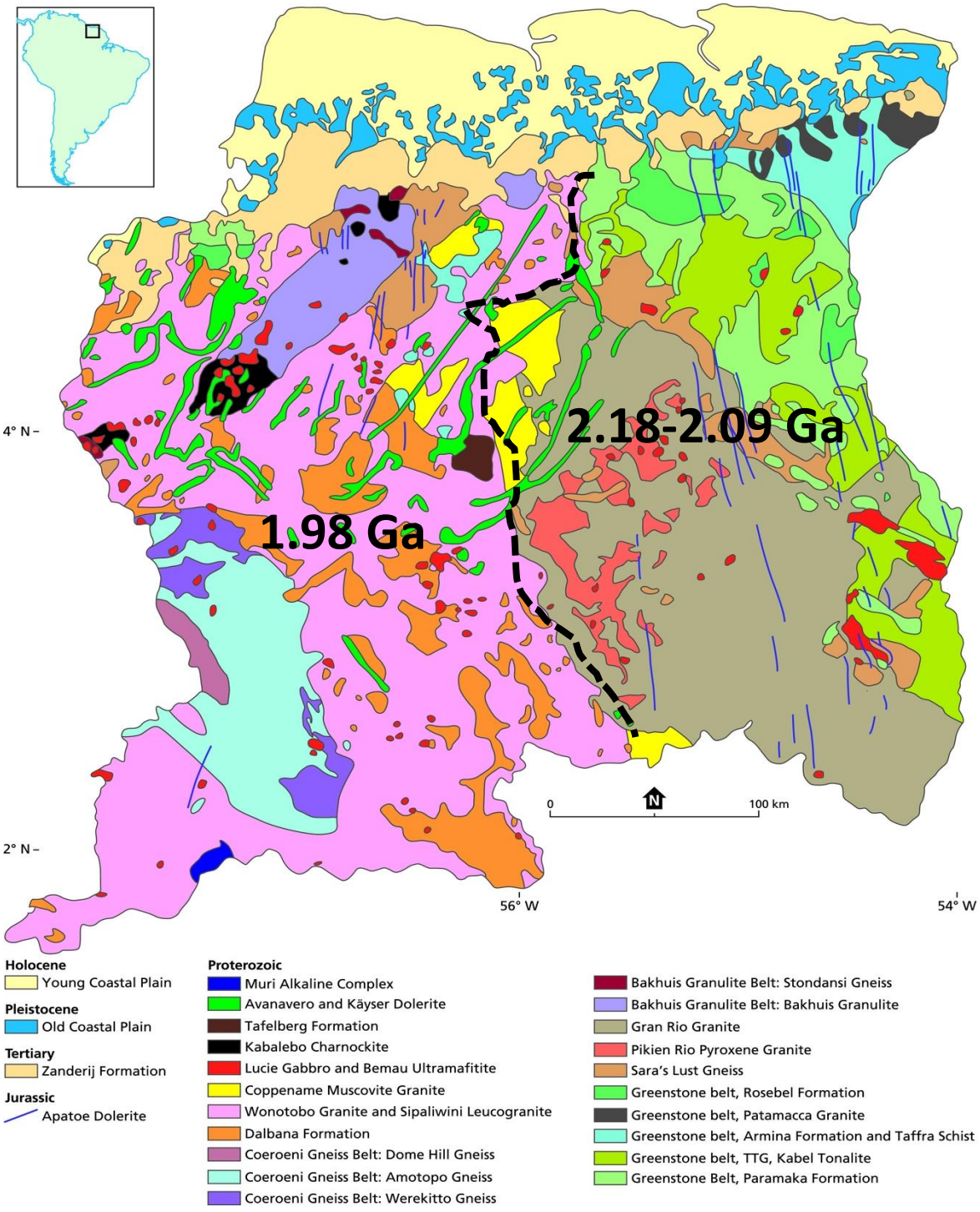

Fig. 1.1: A simplified geological map of Suriname (Kroonenberg et al., 2016).

The former De Goeje Gabbro bodies are indicated here as Lucie Gabbro and Bemau Ultramafitite (in red). The dashed line gives the division of the Guiana Shield in a western and eastern region.

1.2. Motivation, research question and hypothesis

The motivation for this research comes from the unpublished WOTRO project results which were manually analyzed. Nowadays there are several computer programs for the petrogenesis and geochemical data analysis.. De Roever & Bosma (1975, in Kroonenberg et al., 2016) suggested already that the Bemau-type bodies should not be included in the De Goeje Gabbro. To avoid confusion the name De Goeje Gabbro was abolished and Bemau Ultramafitite for those in the greenstone belt in the east, and Lucie Gabbro for the younger suite in the west were introduced.

Research question

What is the origin of the gabbroic-ultramafic bodies in the Guiana Shield of Suriname?

The research question is divided in:

1. Is there a geochemical distinction between the two generations of gabbroic-ultramafic bodies?
2. If yes, did they originate from different magmas, and what is their geologic significance of the two suites

Hypothesis

The recent researches suggested, according to the geological map (fig.1.1), that the gabbroic-ultramafic bodies of Suriname represent two different types of bodies. According to this map a hypothetical border is considered (the dashed line in fig. 1.1), separating the western granitoid regions and the eastern greenstone belt.

1.3. Aim and objectives

This research aims to define the geological, petrological and geochemical characteristics of the gabbroic-ultramafic bodies spread over the Guiana Shield in Suriname. The data were gathered during a WOTRO project in 1977, also the geochemical data, INAA, XRF analysis are from this previous research. This thesis is a geochemical analysis based on statistical data processing using SPSS and petrological interpretations with the computer program GCDkit and Past3. The analyses should help to answer the sub questions of this research. It will indicate whether the gabbro-ultramafic bodies in Suriname are originated from one type or different types of magma and their geologic significance.

1.4. Outline of the thesis

The research is divided into four phases. The first phase is creating a digital database, followed by the second phase with comprehensive descriptions of the acquired data. The third phase includes statistical and geochemical analyses. The final phase describes the interpretations and conclusions about the origin of the gabbroic-ultramafic bodies.

2. Literature Review

For a better understanding of the literature review the nomenclature of gabbros is projected (fig.2.1).

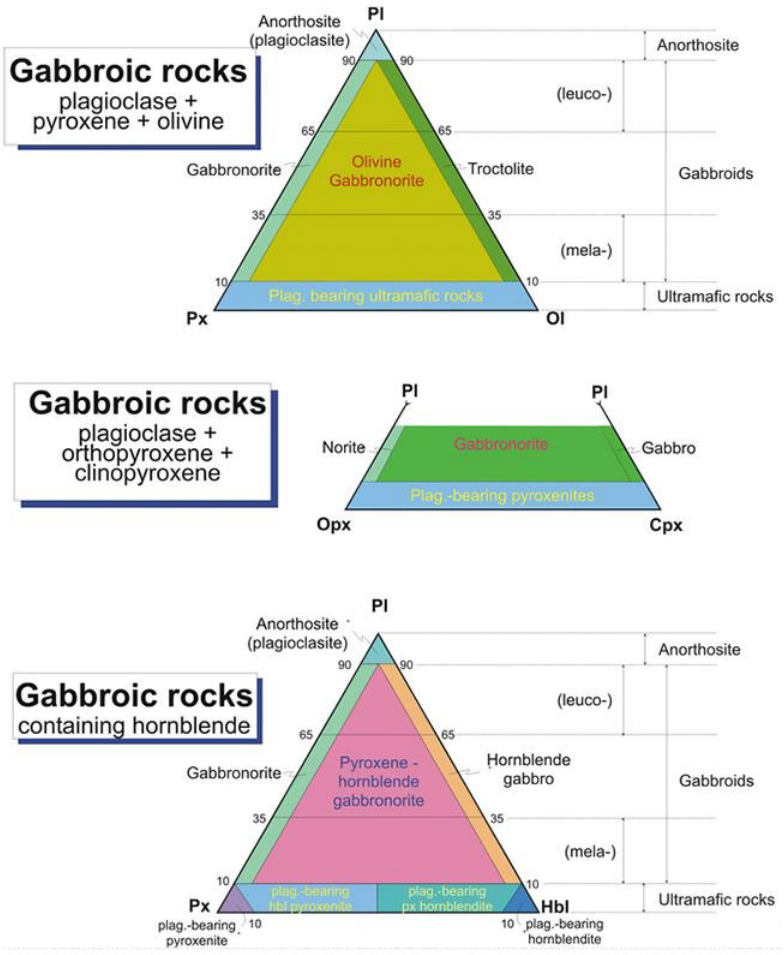

Fig. 2.1: Diagram of gabbroic rocks from IUGS (http://www.alexstrekeisen.it/english/pluto/troctolite.php - 6th of May 2019

2.1. Regional geology: the Guiana shield and the De Goeje Gabbro

The Guiana Shield is a crystalline basement, of mainly Proterozoic age, that lies between the Orinoco and Amazon river basins in northeastern South America. The shield is spread over Eastern Colombia, Venezuela, Brazil and the three Guianas (Guyana, Suriname and French

Guiana) (Gibbs & Barron, 1993). Suriname occupies a central place within the Guiana Shield (Bosma. et al., 1983).

The Shield in Suriname consists essentially of two high-grade metamorphic belts of Lower Proterozoic age, the Falawatra and Coeroeni Groups; a Lower Proterozoic greenstone belt (Marowijne Group) and a vast Lower Proterozoic granitoid-volcanic complex (Bosma et al., 1983). According to Kroonenberg et al. (2016) the greenstone belt is the oldest. The granitoid-volcanic complex consists of four different groups of igneous rocks: (1) deep-level granites, (2) shallow-level granites, (3) acid and intermediate metavolcanic rocks and (4) small gabbroic to ultramafic bodies: De Goeje Gabbro (Bosma. et al., 1983).

According to recent research data the U-Pb zircon age of the gabbros is 2147-2144 Ma in the Tampok gabbro, the continuation of the De Goeje Gabbro in French Guiana, and 1985 ± 2 Ma of the Lucie gabbro in West-Suriname (Kroonenberg et al., 2016).

De Goeje Gabbro: lithology

The De Goeje Gabbro occurs scattered throughout the Precambrian basement. They are numerous metamorphosed gabbroic to ultramafic bodies up to 20 km in diameter. The outcrop shape of these intrusive bodies is circular equidimensional to sill-like. The composition ranges from dunite to pyroxene granodiorite. According to Bosma et al. (1983) drilling and mapping shows vertical and concentric zoning, usually with ultramafic rocks in the lower and inner parts, and gabbronorites or granodiorites in the upper and outer parts of the bodies. Cumulate textures are common, particularly in ultramafic rocks. The minerals that occur are olivine, orthopyroxene and magnetite. Hornblende biotite and calcic clinopyroxene are the main intercumulus minerals of the De Goeje Gabbro. This suggests that the compositional variation of the De Goeje Gabbro resulted

from differentiation of a gabbroic magma, which is upholded by geochemical data (Bosma & Lokhorst, 1975; Veenstra, 1978; Bosma et al. in Bosma et al. 1983). The gabbronorite and ultramafitite bodies are intrusive into the metamorphic complexes. In the granitoid complex they display hybrid dioritic border zones, granites, so that they are considered to be slightly older than the main phase of granitoid magmatism (Bosma & Lokhorst, 1975; De Roever, 1975b in Bosma et al. 1983).

Bosma et al. (1983) suggests that the De Goeje Gabbro was formed by fractional crystallization from a hydrous gabbroic magma with high-alumina basalt affinities. The trend which can be followed of the De Goeje gabbro is a calc-alkaline differentiation trend. Bosma et al. (1983), once more, suggests that these gabbroic bodies resemble the zoned ultramafic complexes in Alaska and the Urals, western Colombia and the basic plutons in southern California.

2.2 Analogues of the De Goeje Gabbros and the ultramafic bodies

The Alaskan/Ural-type mafic-ultramafic intrusions

The Alaskan/Ural-type intrusions are ultramafic-mafic zoned intrusions in orogenic belts, without large intrusions (Pettigrew & Hattori, 2006). The Alaskan/Ural-type intrusions are smaller than other types of mafic-ultramafic igneous complexes. They are structured as small circular or elliptical geometry, linear array of clustered stocks, crude concentric lithological zonation grading from an olivine-rich ultramafic core to a more differentiated mafic margin (Yuan et al. 2017). Cores consist of dunite, wehrlite, olivine clinopyroxenite, clinopyroxenite, hornblende clinopyroxenite, clinopyroxene hornblendite or hornblende- and/or clinopyroxene-bearing gabbro/diorite. There is a dominance of clinopyroxene and hornblende in the composition, a

scarcity of orthopyroxene and plagioclase, as well as the enrichment in light rare earth elements and depletion in high field strength elements.

The LILE[1] of this intrusion is high with lower value of Nb, Ta and Ti. This indicates that their parental magmas are from a depleted mantle source that has undergone metasomatism in a subduction setting. The Alaskan/Ural type intrusions show negatively sloped REE patterns without Eu anomalies. The lack of Eu anomalies explain that plagioclase has an suppressed crystallization in the hydrous parental magma. It may also explains the fact that the parental magma is oxidized, because all REE including Eu are trivalent in an oxidized melt. Olivine is Mg-rich and clinopyroxene is diopside in these intrusions. Clinopyroxene are also characterized by low Ti contents and low Al in tetrahedral sites (Yuan, et al., 2017).

The parental magmas for the Alaskan/Ural-type intrusions were picritic[2] and hydrous, with arc tholeiite affinity. They are limited to late-Precambrian and Phanerozoic orogenic belts. The Alaskan/Ural-type intrusions probably intruded during the end fase of the intra arc basin (Pettigrew & Hattori, 2006). According to Yuan, et al. (2017) the ultramafic-mafic intrusions of the Precambrian in the Zhongtiao mountain region, North China Craton span from komatiitic to basaltic fields on the Jensen diagram. The trend on the TiO_2 vs FeO^{tot}/MgO diagram evidence a from the tholeiitic evolutionary. The Alaskan-type ultramafic-mafic intrusions in the Zhongtiao mountain region, North China Craton involve a Mg-rich hydrous parental magmas and subsequent crystal fractionation-accumulation processes. The determination of parental magma composition is done using maximum MgO contents of clinopyroxene and the partition coefficient of Mg between clinopyroxene and melt can result in a high MgO estimate of > 12 wt%. The

[1] LILE: large-ion lithophile elements; incompatible element. During the fractional crystallization of magma and magma generation by the partial melting of the eath's mantle and crust, elements that have difficulty in entering cation sites of the minerals are concentrated in the melt phase of magma.

[2] Picrite: a variety of olivine-diabase without feldspar

hornblende-rich petrographic character and hornblende-bearing pegmatites provide tangible testaments to the hydrous nature of the parental magmas (Yuan et al., 2017).

The mafic-ultramafic intrusion in the Hengshan area (Wang, et al., 2010) are typical of subduction-related magmas. The parental magma likely originated from the depleted mantle wedge above a subduction zone, and experienced fractional crystallization of olivine and clinopyroxene.

3. Data collecting and analyses

The geochemical data used for this research have been obtained in the 1980's on rock samples collected by the Geological and Mining Service (GMD).. This chapter describes the chemical analyses (INAA and XRF) and gives a description of the places from where the samples were taken. The chemical data obtained from the analyses are first of all digitalized. The data were till now only available as paper print outs. The samples have a GMD code and a code for indicating the location of the sample (attachment 1, database). According to map (fig.1.1) Sample locations are divided in an eastern and a western region. Table 3.1. displays the division of the sample locations.

Table 3.1: the sample locations according to the division in the eastern and western region of the gabbros and the code used in this study.

#	East	Code	#	West	Code
1	Awalape	Awa	1	Adampada	Ada
2	Gran Rio	GR	2	Bakhuis west area	BHW
3	De Goeje Gabbro	DGJ	3	Coeroeni area	Coe
4	Oelemari	Oel	4	Emma	Emm
5	Paramaka	Para	5	Hebiwerie	HbW
6	Pique	Piq	6	Kabalebo	Kabo
7	Bemau	Bem	7	Lucie Monding	LuMo
8	Upper Saramacca	Sara-up	8	Maskita	Mask
			9	Marataka	Mrt
			10	Sipaliwini	Sip
			11	Stontabriki	Ston

3.1. The Chemical Analyses

The INAA

The **Instrumental Neutron Activation Analyses (INAA)** on 87 samples from 19 gabbro bodies were performed by the Inter-University Reactor Institute at Delft (IRI) in 1974, 1977 and 1979. From each sample two small volumes, 1 cm^3, have been analysed separately.

The **INAA** has been an important tool in trace element studies of geological materials. Samples need not be treated chemically either before or after treatment, and matrix problems associated with the physical nature of the material are absent. The main task of the analyst using INAA is to identify the many radionuclide's that can be produced in these complex materials. At least ten and sometimes as many as sixteen elements can be determined following a single irradiation. The detection limit of many elements is less than 1 ppm and the precision typically ranges from 0.1 to 1 ppm. The two major requirements are access to a reactor with a flux of $1x10^{12}n.cm^{-2}.s^{-1}$ and suitable counting equipment (Gibson & Jagam, 1980).

The XRF analyses

X-Ray fluorescence (XRF) analyses on 29 samples from 12 mafic-ultramafic De Goeje bodies , for 11 major elements, were performed by Mr E. Murray at the Laboratory of the Geological and Mining Service of Suriname (GMD. It works on wavelength-dispersive spectroscopic principles. The XRF is typically used for bulk analyses of major elements of geological materials. The analysis of major and trace elements in geological materials by x-ray fluorescence is made possible by the behaviour of atoms when they interact with radiation.

3.2. Petrographical description

This paragraph describes the data analyses and the petrography of the samples from the several locations, divided regions. The petrographical description is from the Bosma, et al., 1980 (unpublished) report.

The Western region

Adampada

The Adampada body is a rather small pluton (4x9km^2) occurring at the SE boundary of the Bakhuis mountains, largely surrounded by older high-grade country rock, charnockitic granulites mainly, and fault-bounded at its SE side. The lateritic soil covering the ultramafic part of the body is Ni-enriched (Oosterbaan in Bosma et al., 1980). The petrology of Adampada consists for a small part of an ultramafic olivine-rich cumulate, mainly wehrlite with locally olivine melagabbro; a scanty intercumulate is formed of plagioclase and biotite. The larger part of the body is made up of pyroxene hornblende gabbronorite and notably of leucogabbronorite, including very rare anorthosite. Both rocktypes are equigranular and medium-grained (3-4mm).

Bakhuis West

Some fifteen gabbronoritic plutons, 0.5 – 25 km^2 in size, occur in the southern part. The occurrences are divided over regions 4 and 5 (gabbronorites within pyroxene granites) and region 6 (gabbronorites occurring within strongly cataclastic biotite granites). The modal pluton has a compositional range from rare olivine-bearing gabbronorite over (leuco-)gabbronorite to pyroxene (monzo-)diorite. The crystallization sequence is olivine, a cumulus component, plagioclase, ortho- and clinopyroxene, rare intercumulus hornblende, intercumulus biotite, interstitial quartz and microcline. Olivine, a rare cumulus mineral, is occasionally accompanied by green spinel.

Coeroeni area

Four moderate sized bodies (up to 10 km^2) and more than a dozen small occurrences of ultramafic and gabbro-dioritic intrusive were found within the high-grade gneisses underlying the area on both sides of the Coeroeni river. Notably the larger bodies form prominent laterite-capped hills and coincide with positive aeromagnetic anomalies (butterfly pattern) up to 6000 gammas. All bodies, large and small show some metamorphism. Ultramafitite was not found together with gabbro-diorite in the same body. Non- to slightly metamorphic ultramafitites are: hornblende bearing websterite, consisting of about equal amounts of medium-grained ortho- and clinopyroxene and some hornblende; and olivine-bearing pyroxene hornblendite, consisting mainly of poikilitic coarse-grained light-brown to green hornblende. Most ultramafic rocks in the Coeroeni area are altered into schists or non-oriented rocks consisting of clinochlore, serpentine, talc and tremolite in varying amounts. The gabbronoritic to dioritic intrusive bodies have a number of distinctive features in common; they are commonly melanocratic rocks consisting usually of euhedral orthopyroxene, clinopyroxene and plagioclase, brown-green hornblende and reddish brown biotite, the northern occurrences of the Coeroeni are.

The gabbronoritic intrusive in the Sisa-Creek belong, at least in part, to the Bakhuis-West occurrences, all have trace-element patterns conforming to early plagioclase cumulates. Some samples are green-spinel bearing olivine gabbronorites, typically leucocratic plagioclase cumulates. They are almost without hornblende.

Hebiweri

The Hebiweri mountain, 450m in height, is situated as an isolated hill at the left bank of the Coppename river, in a low relief landscape underlain by biotite granite. The mountain itself is

underlain by a fairly large (25km^2) gabbroic intrusion, a differentiated body with troctolite as its most basic member grading to leuco(gabbro)norite.

Kabalebo

A few small ultramafic to dioritic intrusive bodies occur in a limited area at the SW margin of the Bakhuis mountain complex about 8km NE of Kabalebo airstrip, W of the Kabalebo river.

The bodies are emplaced in partly magmatic banded pyroxene gneisses and pyroxene amphibolites (the Falawatra complex), some country rock metasediments exhibit pyroxene hornfels metamorphism, as known from drillings. Country rock and intrusive bodies are both in contact with –preasumably younger- pyroxene (bearing) granites. It is rather difficult to make a strict separation between the pyroxene granitoids and the intermediate pyroxene quartz diorites supposed to belong to the mafic-ultramafic intrusions.

The largest body, represented at the surface by a gabbronorite and some pyroxene quartz diorite samples, is reported to be marked by both aeromagnetic and EM-anomalies. Drillings into this body revealed the subsurface presence of ultramafic rocks: olivine pyroxene hornblendites mainly with an occasional pyroxene hornblende peridotite or olivine hornblende pyroxenite. It would seem from the drillings that the hornblendite is surrounded by leucocratic pyroxene quartz diorite, and that both rock types are intruded by granite and granitic veins. Light brown biotite is a rock forming mineral in most hornblendites.

Lucie Monding

The Lucie monding intrusion, of almost circular outline, measuring about 10 km^2, is situated at the confluence of the Coeroeni and Lucie rivers, and consists mainy of melanocratic gabbronorite to diorite. The country rock consists of amphibolite facies biotite gneiss. The intrusion contains many xenoliths, ranging from handsize rounded fragments to angular slabs of some metres in

outline, which are in part fragments of biotite gneiss but largely consisting of micro gabbro, presumably representing disrupted parts of a chilled margin. The body is traversed by veins of varying mineralogy. An ultramafic component has not been encountered in the Lucie monding body. The most mafic component is a melagabbronorite consisting of 35% euhedral crystals (2-3mm) of pyroxene (30% opx – 5% cpx), 30% euhedral to subhedral plagioclase (63% An). The melanocratic gabbronorite grades into a pyroxene hornblende biotite diorite.

Maskita

A butterfly aeromagnetic anomaly coinciding with an EM-anomaly marks the position of a small gabbronorite-ultramafitite enclave surrounded mainly by megacryst-bearing biotite muscovite granite, along the W bank of the Maskita creek. Drilling has revealed the presence of a differentiated body consisting of hornblende peridotite, hornblende pyroxenite and biotite hornblende (mela)gabbronorite. Some cordierite biotite hornfels occurs in the drillings in contact with ultramafitite.

Marataka

The presence of a mafic body below a cover of Tertiary sands in the Maratakka area is indicated by a pronounced aeromagnetic “butterfly” anomaly in the area N of the Bakhuis mountains, somewhat E of the Maratakka creek. Test drilling showed the anomaly to coincide with a body of essentially leuconoritic to pyroxene dioritic composition, which locally contains cordierite hornfels metasedimentary xenoliths. The pyroxene diorite may pass into pyroxene (mela)granodiorite. The body seems to be surrounded by muscovite biotite granites which also occur as veins in the mafic rocks. The Maratakka body is petrologically very similar to the Bakhuis area leuco(grabbro) norites, it consists predominantly of hornblende-free biotite quartz norite to pyroxene quartz diorite passing locally into pyroxene tonalite to melagranodiorite.

Quartz and microcline may be introduced into the mafic rocks during the emplacement of the surrounding granites.

Sipaliwini

The area on both sides of the upper course of the Sipaliwini river is mainly underlain by low-grade acid metavolcanics (presominantly ignimbrites), and several types of granitoids, biotite granites, granophyric granites, alaskites, intruding the metavolcanics, in the biotite granites such bodies occur as enclaves. Some hornblende (mela)tonalities occurring in the adjacent amidst low-grade metavolcanics, probably also belong to these De Goeje bodies. A single ultramafic body, a hornblendite was found amidst metavolcanics. The one ultramafitite is an olivine pyroxene hornblendite. The hornblendite is partly altered into an epidote-zoisite-actonolite rock. The gabbros and diorites are melanocratic to mesocratic fine- to medium grained hypidiomorphic granular rocks. In most rocks, green hornblende is the dominant mafic mineral.

Stontabriki

Four very small mafic bodies consisting of pyroxene biotite hornblende diorite/gabbro, biotite hornblende pyroxene (mela-)gabbro and ultramafitite, occur as enclaves within a tonalite body emplaced between metasediments and biotite muscovite granites. The area is situated NE of Stontabriki (=stone island) in the Coppename river. Rather weak aeromagnetic anomalies, not quite coinciding with EM anomalies, mark the mafic enclaves. Drilling has revealed a normal layering and gradual differentiation sequence (possibly with graded igneous layering) of ultramafitite-melagabbronorite-gabbronorite in one drillhole. In other drill holes diorites occur above and below the (mela)gabbronorite. The diorite locally contains ultramafic xenoliths. The tonalite locally has intruded in the ultramafitite. The neighbouring granite is present as veins both in the tonalite and in the mafic-ultramafic rocks. Gabbronorite is the dominant rocktype in the

drillings from the largest mafic body, diorite constitutes about 15% of the drillings, and about 10% of the recovered cores consist of ultramafitite. The ultramafitite is a hornblende pyroxene peridotite to olivine hornblende pyroxenite. The gabbronorites are biotite hornblende pyroxene melagabbronorites (melanorites locally) to pyroxene biotite hornblende gabbronorites and meladiorites. Most gabbronorites are olivine bearing. Low grade static alterations are also fairly common in all rock types mentioned: olivine, pyroxenes and primary hornblende are replaced by serpentine, talc, tremolite and actinolite.

The Eastern Region

Awalape

Several small plutons, mainly gabbronorites to diorites, occur within granitoid rocks along the Upper Tapanahony river. The largest body ($3x5km^2$), mainly a gabbronorite, is situated near the confluence of the Awalape creek and the Tapanahony; a small ultramafic body was found at Loth falls; a mainly dioritic body is situated at Mauricius falls. The Awalape occurrence is characterized by a strong positive magnetic anomaly and covered by a lateritic soil with Ni- and Cu contents. The Loth falls ultramafitite is a hornblende pyroxenite consisting of rather small augite crystals surrounded by larger poikilitic hornblende. The Awalape gabbronorite is a fine- to medium grained biotite and hornblende bearing olivine pyroxene gabbronorite to biotite bearing pyroxene hornblende gabbronorite. The diorites are mainly pyroxene bearing biotite hornblende diorites to quartz diorites; all mafic bodies are surrounded by younger granitoid rocks, and are consequently more or less strongly altered.

GranRio

One large and several fair sized intrusive mafic bodies, emplaced within acid metavolcanics and within high-grade gneisses, are found along the upper course of the Gran Rio river. Country rocks

and intrusive bodies are both intruded by various biotite granites. From these Gran Rio occurrences some mela gabbronorite samples and one gabbronorite are known. The average mela gabbronorite is a cumulate of olivine and pyroxenes and locally plagioclase; greenish brown hornblende is a common late inter cumulus mineral (5-20%) in all samples; biotite is present in smaller amounts (1-5%); primary magnetite is usually present/

De Goeje Gabbro

Ten large to very large intrusive gabbronorite-diorite bodies (up to 200 km^2) constitute a topographically pronounced ridge of laterite-capped hills, known as the De Goeje Mountains, striking SE across the Lawa river in SE Suriname and the adjacent part of French Guiana. The bodies, although among the largest basic intrusions known from the northern Guiana shield, do not coincide with strong aeromagnetic anomalies. The country rocks are metavolcanics and metasediments of the geosynclinals Marowijne Group, the metamorphic aureoles locally exhibit pyroxene-hornfels parageneses. The De Goeje bodies are described by IJzerman as consisting of rare troctolite and common olivine-rich gabbronorite and norite grading over olivine-bearing hornblende biotite pyroxene gabbronorite to quartz-bearing pyroxene biotite hornblende gabbro and diorite without olivine.

Oelemari

One of the largest mafic intrusions in SE Suriname occurs SE of Oelemari airstrip, it stretches ESE parallel to the general strike of its high-grade biotite gneiss country rock, almost reaching from the Oelemari creek to the Loë Creek. Some smaller bodies occur in the neighbourhood.

Pique

A fairly large ultramafic-mafic body underlies the Pique hill in NE Suriname. The body is intrusive in the geosynclinals metavolcanics and metasediments of the Paramakka Formation. Some chromite float occurs in the lateritic soil covering the ultramafic part of the body. The pique ultramafics are mainly pyroxenites and websterites, primary magnetite is of frequent occurrence, enclosed in pyroxenes or olivine (cf the Bemau ultramafitites). The rocks are in part affected by low grade alteration resulting in e.g. tremolite rocks.

Bemau

Two fairly large ultramafic bodies (up to 15km^2) and some smaller bodies, with subordinate gabbroic to dioritic rocks which commonly bear ovoid ultramafic inclusions, occur along the Saramacca river, between the Bemau hill and the Dramhosso falls. The ultramafics are apparently intrusive in a banded series of amphibolites and quartzo-feldspathic gneisses, as well as in the metavolcanics and metasediments of the Marowijne Group (Bosma et al.. 1978), whereas leucotonalitic granitoids have discordant intrusive contacts against the ultramafic bodies. The larger part of the bodies is thoroughly altered by low-grade metamorphism. The petrography of the unaltered ultramafics can be studied from some drill-core samples. The dark grayish ultramafitites are described by Veenstra (1983) as a, putatively gradational, series of: dunite, wehrlite, olivine clinopyroxenite to clinopyroxenite, and websterite to hornblende pyroxenite.

The gabbro-diorites are commonly dark green medium-grained rocks, consisting of brownish green to light green or locally blue-green amphibole and plagioclase with subordinate quartz, biotite and clinopyroxene. Most ultramafics are thoroughly altered, occurring as schists and rocks of tremolite, serpentine, clinochlore, carbonate and talc in varying proportions. The gabbros and dolerites are commonly metagabbros and metadiorites.

4. Geostatistic results

This chapter presents the results of several geostatistical analyses of the data, such as the descriptive statistics, correlation, principal component analyses, cluster analyses and discriminant analyses, in order to distinguish the eastern and western gabbroic bodies on the basis of their geochemistry.

4.1. Geostatistics of the elements as analyzed with XRF

Table 4.1: Descriptive statistics of the XRF data set

	Minimum	Maximum	Average	Std. deviation	Skewness - sd = 0.35	Kurtosis - sd = 0.69
SiO2	39.18	88.76	52.65	10.91	**1.78**	**2.84**
Al203	3.64	24.52	12.91	4.48	-0.26	0.03
Fe203	0.00	25.79	10.90	5.54	0.07	0.91
MgO	0.00	29.92	9.96	7.78	0.81	0.08
CaO	0.13	15.45	8.02	4.10	-0.54	-0.35
Na2O	0.42	8.83	2.51	1.92	**1.49**	**2.17**
TiO2	0.07	2.16	0.79	0.54	0.84	0.11
K2O	0.02	3.50	0.73	0.86	**1.88**	**3.14**
MnO	0.00	0.40	0.16	0.08	-0.17	1.36
P205	0.01	0.62	0.15	0.16	**1.58**	1.77
Cr203	0.00	0.41	0.08	0.11	**1.59**	1.59

None of the elements have an extreme skewness. The skewness of the normal distribution is 1.00. The skewness of SiO_2, K_2O, P_2O_5, Cr_3O_2 and Na_2O are high. The kurtosis SiO_2, K_2O, and Na_2O are also high.

Table 4.2:The correlation of the elements according to the XRF analyses

	Cr2O3	MgO	MnO	Al2O3	Na2O	K2O	SiO2	Fe2O3	TiO2	P2O5	CaO
Cr2O3	1.00	0.92	0.37	-0.76	-0.68	-0.26	-0.29	0.07	-0.53	-0.29	-0.27
MgO	0.92	1.00	0.54	-0.83	-0.80	-0.40	-0.48	0.23	-0.52	-0.38	-0.14
MnO	0.37	0.54	1.00	-0.63	-0.46	-0.43	-0.46	0.54	0.10	0.04	0.06
Al2O3	-0.76	-0.83	-0.63	1.00	0.63	0.12	0.31	-0.34	0.24	0.13	0.16
Na2O	-0.68	-0.80	-0.46	0.63	1.00	0.62	0.66	-0.41	0.46	0.60	-0.26
K2O	-0.26	-0.40	-0.43	0.12	0.62	1.00	0.71	-0.40	0.22	0.60	-0.53
SiO2	-0.29	-0.48	-0.46	0.31	0.66	0.71	1.00	-0.79	-0.09	0.39	-0.40
Fe2O3	0.07	0.23	0.54	-0.34	-0.41	-0.40	-0.79	1.00	0.45	-0.09	0.11
TiO2	-0.53	-0.52	0.10	0.24	0.46	0.22	-0.09	0.45	1.00	0.53	-0.01
P2O5	-0.29	-0.38	0.04	0.13	0.60	0.60	0.39	-0.09	0.53	1.00	-0.44
CaO	-0.27	-0.14	-0.06	0.16	-0.26	-0.53	-0.40	0.11	-0.01	-0.44	1.00

There are three main groups of correlations. The first group consists elements which are highly correlated. The groups (MnO, MgO and Cr_2O_3) and (Al_2O_3 and Na_2O) have high positive correlation with each other and high negative correlation with the elements of the other group. So if there are relatively many elements of one group in a rock then there are relatively few of the other group and vice versa. The second group consists of SiO_2, K_2O, and Fe_2O_3 where K_2O and SiO_2 have a positive correlation with each other and a high negative correlation with Fe_2O_3. Furthermore, K_2O and SiO_2 are correlated with Na_2O, but less with P_2O_5, while they are reasonably high negative correlated with MgO, MnO, and CaO. The third group consist of TiO_2, P_2O_5 and CaO. TiO_2 and CaO are not correlated.

The principal component analysis of major elements according to XRF analyses

The procedure

PCA is a feature extraction method that uses orthogonal linear projections to capture the underlying variance of the data.

1. The first principal component is just the normalized linear combination of the variables that has the highest variance.
2. The second principal component produces a linear combinations or dimensions of the data that are really high in variance and that are uncorrelated.

A method to determine the number of principal components is to look at the scree plot (fig. 4.1a). The number of components is determined at the point beyond which is the remaining eigenvalues are all relatively small and of comparable size. Figure 4.1 shows that the XRF data elements have four Principal Components: PC1, PC2, PC3 and PC4.

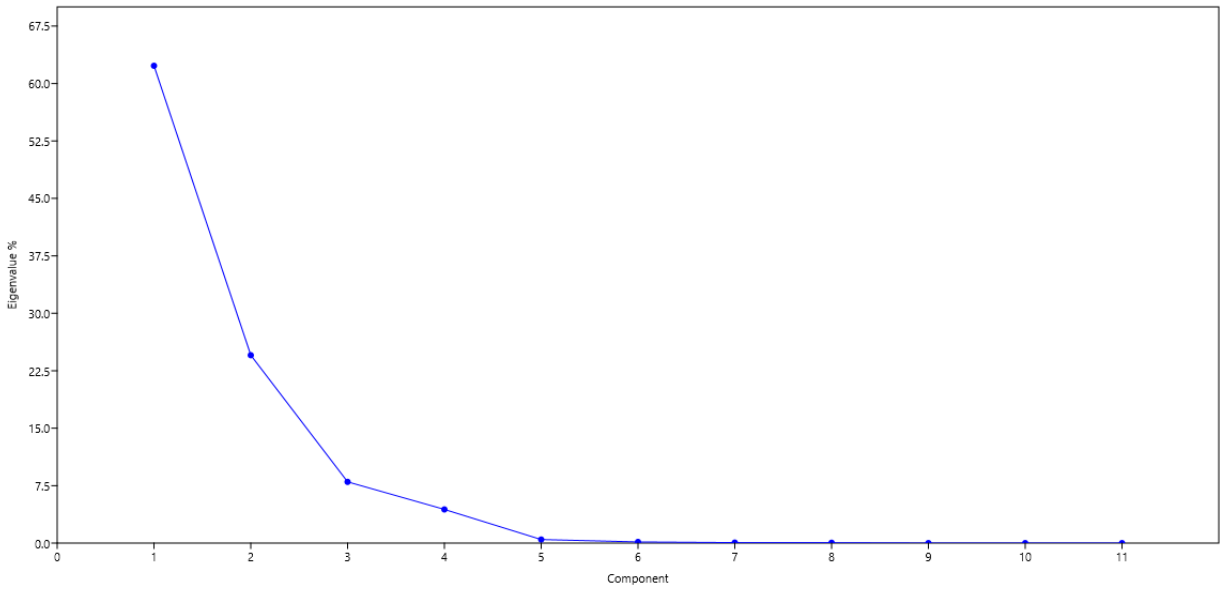

Fig. 4.1: scree plot of the pca of the elements based on XRF analyses

Table 4.3: The loadings of the 4 components of the XRF data elements

	PC 1	PC 2	PC 3	PC 4
Na_2O	0.10	-0.02	-0.09	0.03
MgO	-0.74	-0.37	0.29	0.28
Al_2O3	0.46	0.28	0.42	0.62
SiO2	0.41	-0.64	-0.27	-0.18
P2O5	0.01	-0.00	-0.03	0.01
K2O	0.05	-0.07	-0.13	-0.01
CaO	0.00	0.27	0.53	-0.71
TiO2	0.02	0.05	-0.10	-0.02
Cr2O3	-0.01	-0.01	0.00	0.01
MnO	-0.00	0.00	-0.00	-0.00
Fe2O3	-0.26	0.55	-0.59	0.02

According to table 4.3, the first principal component increases with a decrease of MgO. The second component increases with a decrease of SiO_2 and increase of Fe_2O_3, thus if SiO_2 increases, Fe_2O_3 will be decreasing. The third principal component increases with the decrease of Fe_2O_3 and increase of CaO. The fourth principal component increases with a decrease of CaO and increase of Al_2O_3, by decreasing of CaO, Al_2O_3 will increase.

Figures 4.2 till 4.7 displays the scatterplot of the four components of the PCA. The plot PC3 shows almost a clear distinction between east and west. PC3 is responds with the increase of CaO and decrease of Fe_2O_3.

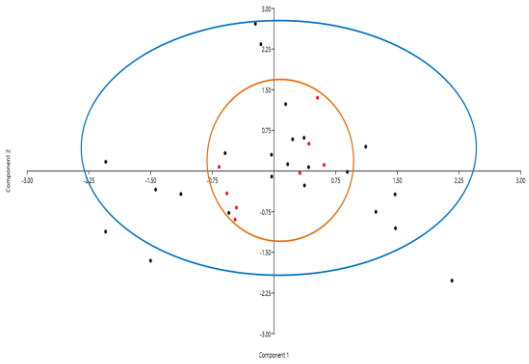

Fig. 4.2: pca plot of the XRF data elements between pc 1 (x-axis) and 2 (y-axis

)

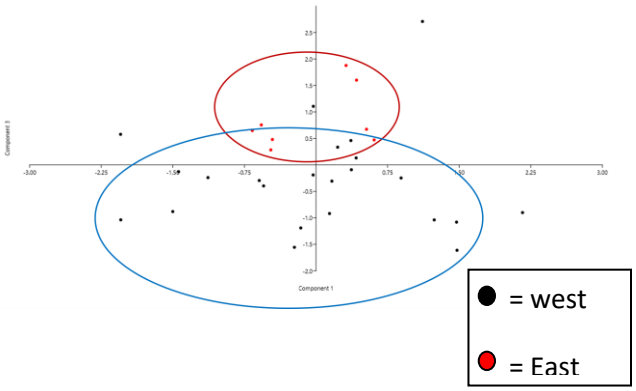

Fig. 4.3: pca scatter plot of the XRF data elements between pc 1 (x-axis) and pc 3 (y-axis)

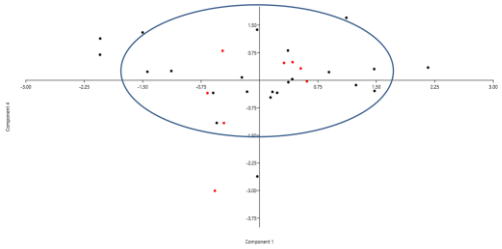

Fig. 4.4: pca scatter plot of the XRF data elements between pc 1 (x-axis) and pc 4 (y-axis)

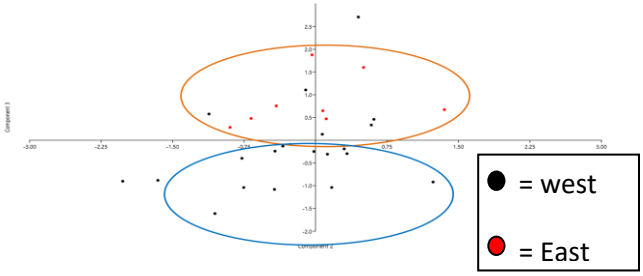

Fig. 4.5: pca scatter plot of the XRF data elements between pc 2 (x-axis) and pc 3 (y-axis)

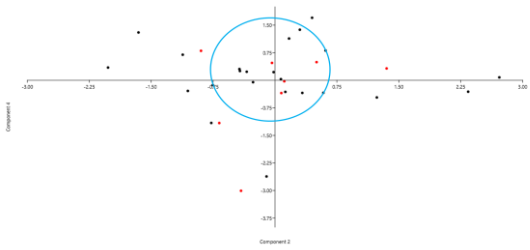

Fig. 4.6: pca plot of the XRF data elements between pc 2 (x-axis) and pc 4 (y-axis)

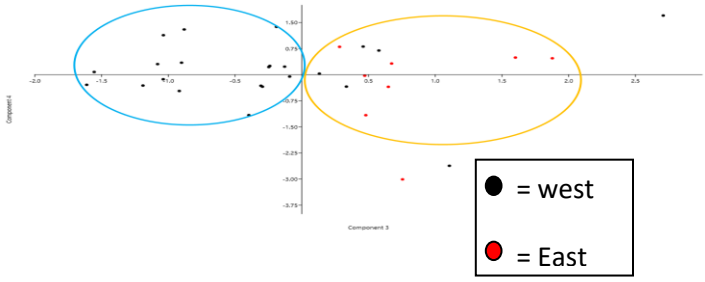

Fig. 4.7: pca scatter plot of the XRF data elements between pc 3 (x-axis) and pc 4 (y-axis)

Cluster analyses of the elements according to XRF analyses of east and west

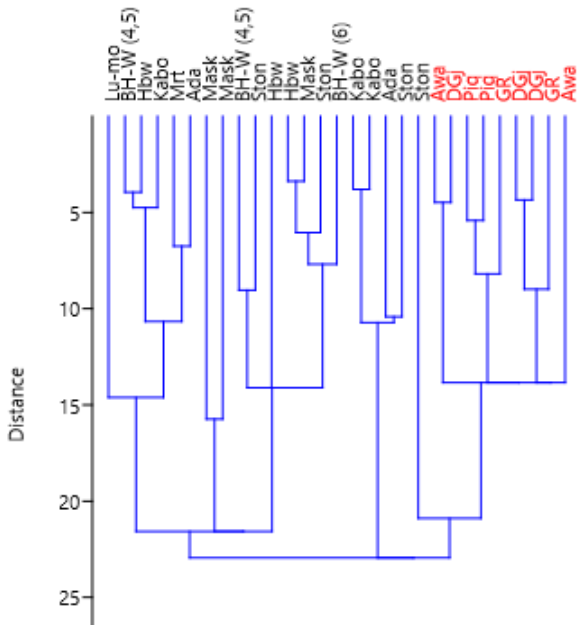

Fig. 4.8: The dendrogram of the elements according to the XRF analyses using centroid linkage clustering method of east and west

The dendrogram (fig. 4.8) does not show a clustering between XRF elements of east and west.

4.2. Geostatistics of the elements as analyzed with INAA

Table 4.4 The univariate statistics of the elements according to the INAA analyses

	N	Mean	Std.deviation	Missing	
				Count	Percent
Sc	87	28	14	0	0.0
Mn	87	1501	455	0	0.0
Fe	87	8181	26096	0	0.0
Co	87	71	40	0	0.0
Cr	86	912	1306	1	1.1
Na	86	12736	8383	1	1.1
Al	86	69328	35995	1	1.1
La	86	10	12	1	1.1
Mg	84	81142	62661	3	3.4
V	84	227	196	3	3.4

Yb	79	1.4	1.1	8	9.2
Eu	78	3	19	9	10.3
Ti	77	5405	3159	10	11.5
Ca	74	70470	22885	13	14.9
Hf	69	2	2	18	20.7
Ni	65	448	4400	22	25.3
Zn	66	84	29	21	24.1
Ce	61	30	29	26	29.9
Lu	51	0.3	0.2	36	41.4
Tb	50	1.0	0.4	37	42.5
Sm	25	4	4	62	71.3
Nd	5	49	16	82	94.3
Dy	4	170	315	83	95.4

The INAA data set contains 87 samples of rock bodies. Five samples with the most missing values are discarded from the data set. The total amount of samples is now 82.

East-west differences: distributions, correlations and regressions

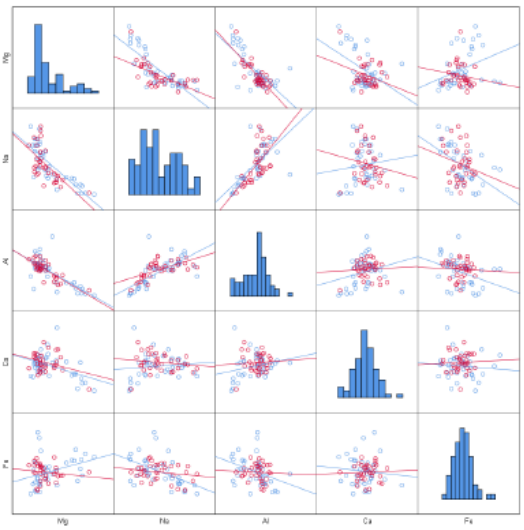

Fig. 4.9: the scatter plots of Mg, Na, Al, Ca and Fe of the INAA analyses. Blue is west, red is east with the regression. The diagonal diagrams shows the distribution of the elements.

Figure 4.9 displays the scatter plots of Mg, Na, Al, Ca and Fe. It is a XY plot of two elements. There is no distinction between the samples of east and west. They are all scattered. But, a group samples from the west is rich of Mg elements, while only one location from the eastern region is

rich of Mg elements. Almost the same trend is identified for Fe. The samples with higher value of Mg has average value of Fe. These elements shows good correlations both positive and negative. The correlation Na with Ca and Mg with Fe is positive in the west and negative in the east.

The principal component analyses of the elements according to INAA analyses

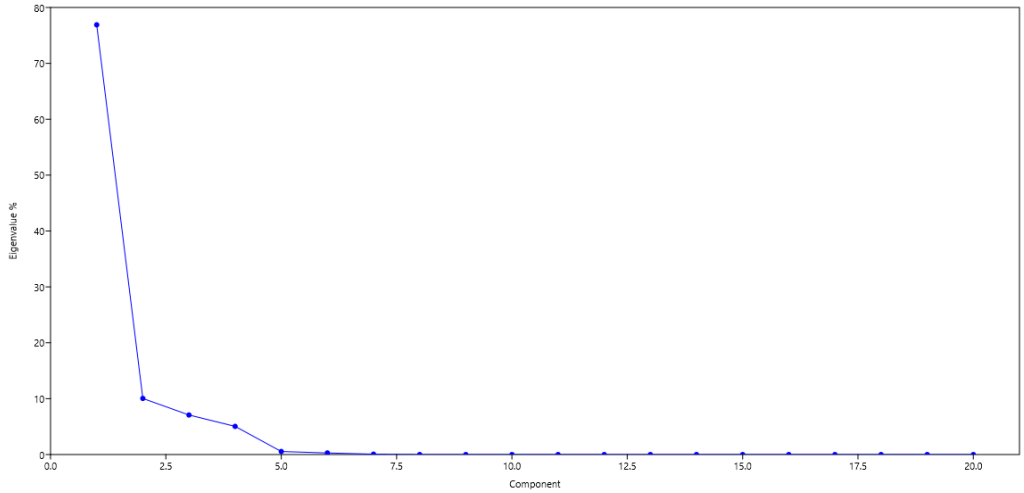

Fig. 4.10: the scree plot of the pca of the elements from the INAA analyses

To interpret each component, the correlations between the original data and each principal component must be computed (table 4.5). The correlation is important at a value greater than 0.50. According to the loadings of the components (table 4.5) shows that pc 1 is strongly correlated with one of the original data. The first principal component increases with increasing the amount of Mg (0.87). The second principal component pc 2 increases with the increasing of Fe (0.89), the third principal component pc 3 increases with the increasing of Al (0.58) and decreasing of Ca (-0.68). This means if Al increases, Ca will be decrease. And the fourth principal component pc 4 correlates with increasing Ca (0.63) and increasing Al (0.67)

Table 4.5. The loadings for 4 components of the elements according the INAA

	PC 1	PC 2	PC 3	PC 4
Na	-0.09	-0.09	0.05	-0.07
Mg	0.87	-0.26	0.15	0.38
Al	-0.45	-0.26	0.58	0.63
Ca	-0.10	0.25	-0.68	0.67
Sc	-3.51E-05	0.00	-0.00	3.86E-05
Ti	-0.02	0.05	0.04	0.00
V	-0.02	0.04	-2.05E-05	0.02
Cr	0.02	-0.01	-0.00	-0.00
Mn	0.00	0.01	0.01	0.01
Fe	0.14	0.89	0.41	0.09
Co	-7.74E-05	0.00	0.00	0.00
Ni	0.00	0.00	0.00	-0.00
Sr	-0.00	-1.06E-05	-6.18E-05	-0.00
La	5.83E-05	-4.76E-05	-2.77E-05	-3.84E-05
Ce	-5.48E-05	-6.15E-05	0.00	-0.00
Eu	-1.85E-05	-2.91E-05	5.23E-05	-0.00
Tb	-3.26E-07	6.0E-07	-2.0E-08	-3.19E-06
Yb	-4.86E-06	3.32E-06	5.08E-06	-1.40E-05
Lu	-4.00E-07	3.81E-07	1.15E-06	-1.54E-06
Hf	-6.69E-06	1.73E-07	1.12E-05	-2.30E-05

The yellow loadings has an amount greater than 0.5

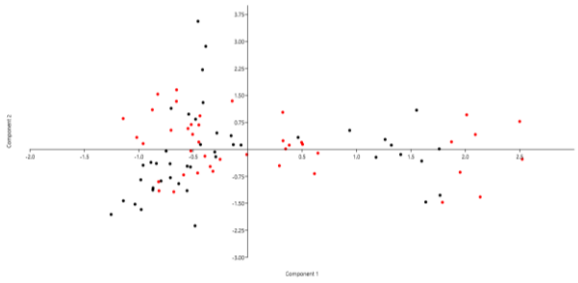

Fig. 4.11: pca plot of the element from INAA between pc 1 (x-axis) and 2 (y-axis)

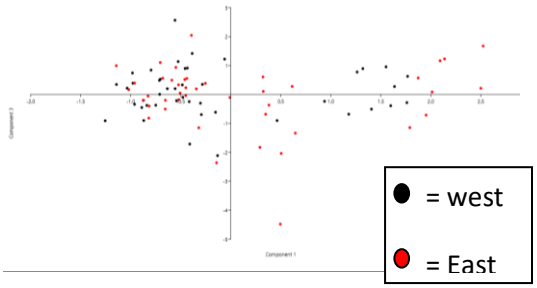

Fig. 4.12: pca plot of the element from INAA between pc 1 (x-axis) and 3 (y-axis)

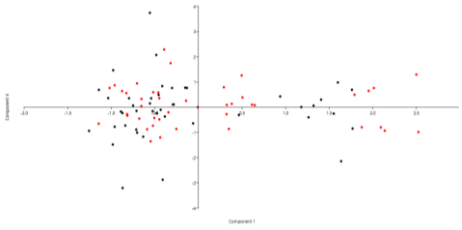

Fig. 4.13: pca plot of the element from INAA between pc 1 (axis) and 4 (y-axis)

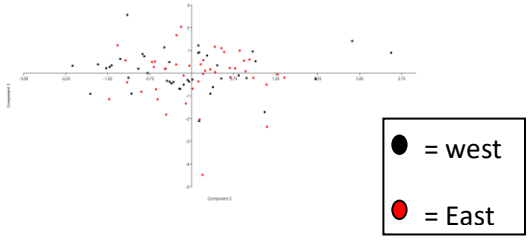

Fig. 4.14: pca plot of the INAA data element between pc 2 (x-axis) and 3 (y-axis)

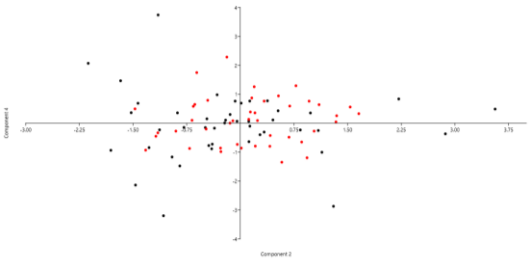

Fig. 4.15: pca plot of the INAA data element between pc 2 (x-axis) and 4 (y-axis)

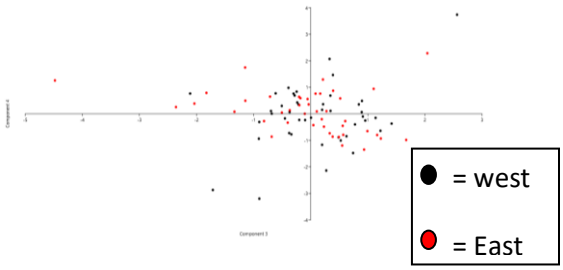

Fig. 4.16: pca plot of the elements from the INAA between pc 3 (X-axis) and 4 (y-axis)

Figure 4.11 till 4.16 displays the pca plot of the INAA element. These plots does not show a distinction in east and west.

Cluster analyses of the elements according to INAA analyses of east and west

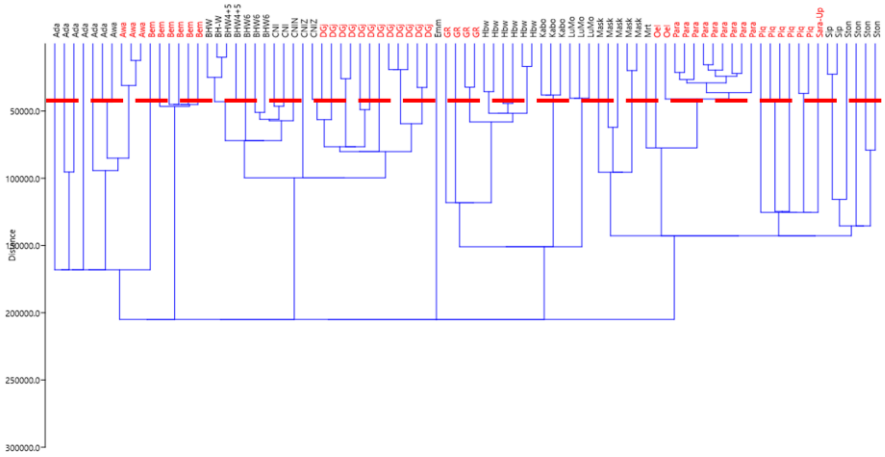

Fig. 4.17: dendrogram of the elements according to the INAA analyses using centroid linkage clustering method.

The dendrogram displays a small clustering (red dashed line) between east and west. The location Bakhuis West, Adampada, De Goeje Gabbro, Paramaka, and Pique shows some similarities.

Discriminant analyses of the samples according to INAA

The response variable for this analysis is east and west. The predictor variables (variables in discriminant function) are: Na, Mg, Al, Ca, Sc, Ti, V, Cr, Mn, Fe, Co and La.

Table 4.6 discriminant analyses of the elements according to INAA

Element	Standardized coefficient of the discriminant function	Correlation between the function and element
Mg	**1.75**	**0.33**
La	**1.08**	**0.29**
V	**0.68**	-0.11
Ca	0.45	-0.18
Na	0.40	-0.10
Co	0.35	**0.36**
Al	0.04	**-0.26**
Sc	-0.32	**-0.31**
Mn	-0.33	-0.17
Fe	-0.16	0.04
Ti	**-0.56**	**-0.26**
Cr	**-0.94**	0.11

The standard weight is compared with the standard regression weight. The samples are divided in east and west. The coefficients give the weights of the regression. Very large values (e.g. Mg: 1.75) indicate the elements sheet of contributions to the prediction based on the function and small values (e.g. Al: 0.04) do not add much. In other words there is no distinction between the East and West samples in their Al content. The last column in the table indicates what the correlations are between the individual elements and the values of the samples on the discriminant function.

Cr with a coefficient of –0.94 shows that it has an important role in the discriminant function, but the samples are scattered. This is possible if all the samples are clustered on one side of the

function. It could also be the other way round, there is no discriminant, but the samples are on the same way in a row as they do in the discriminant function.

Table 4.7 the classification result from the discrimination analyses

			Predicted Group Membership		
		EastWest	West	East	Total
Original	Count	0 West	**27**	5	32
		1 East	4	**25**	29
	%	0 West	**84**	16	100
		1 East	14	**86**	100
Cross-validated[b]	Count	0 West	**21**	11	32
		1 East	9	**20**	29
	%	0 West	**66**	34	100
		1 East	31	**69**	100

a. 85.2% of original grouped cases correctly classified; 67.2% of cross-validated grouped cases correctly classified

b. In cross validation, each case is classified by the functions derived from all cases other than that case.

The procedure

The classification results indicates about the location (east or west) of the sample, just by looking at the value of the elements. To start with the classification, the function is calculated and the value of the sample is determined. Then, for each region, the average is calculated. After this calculation a comparison is made between the calculated average and the value of the sample. If the value of the sample is close to the average of the function in west, than the sample is from the west, for example. For this data set, there are 32 samples from the western region. The discrimination function calculated 27 samples from the west and 5 from the east, according to

the value of the sample. The data set shows 29 samples from the east, but the function calculated only 25 from the east. This explains that 82.2% of the samples are correctly classified.

To ensure the reliability, the discriminant function of all the sample, except for one, is calculated. After the calculation, this specific sample is classified in east or west. This procedure is repeated for each sample. 61 functions are calculated. The results are presented as the cross validation. The classification in west and east is now 67.2% correct. This means that the eastern and western samples are mixed up.

5. Petrogenetic geochemistry results

In this chapter the geochemistry of the gabbros are described. The description of the analyses are according to Rollinson, H. (1993).

The description is done from the **Total Alkalis-Silica (TAS) diagram**. This is the most useful classification scheme available for volcanic rocks. The TAS diagram divides rocks into ultrabasic, basic, intermediate and acid ones on the basis of their silica and alkali metal content (Rollinson, 1993).

The **R1-R2 diagram of De la Roche et al.. (1980)** is also used to analyse the samples. R1-R2 is a classification scheme for volcanic and plutonic igneous rocks based upon their cation proportions, expressed as millications. This diagram is most useful for plutonic rocks. The results are plotted on an x-y bivariate graph using the plotting parameters R1 and R2. R1 is plotted on the x-axis and is defined as: R1 = [4Si – 11(Na+K)-2(Fe+Ti)]

R2 is plotted along the y-axis and is defined as: R2 = (Al+2Mg+6Ca) (Rollinson, 1993)

The **AFM diagrams** of the individual occurrences are also plotted. The AFM diagram is the most popular of triangular variation diagrams and takes its name from the oxides plotted at its apices – Alkalis ($Na_2O + K_2O$), Fe oxides ($FeO + Fe_2O_3$) and MgO. The AFM diagram only indicates the series type (Tholeiite series or Calc-alkaline series).

The element discrimination between the gabbroic rocks is also analyzed. The tasks of trace element geochemistry is to discover which geological processes may have this effect and to quantify the extent of a particular process.

5.1. Geochemistry of the elements according the XRF data

The Western region

According to the TAS diagram (fig. 5.1), the R1-R2 plot (fig. 5.2) and the AFM diagram (fig. 5.3) of the western region the rock samples are spread over the several divisions, but most of them are subalkaline/tholeiitic basic rocks, some ultramafic and gabbros.

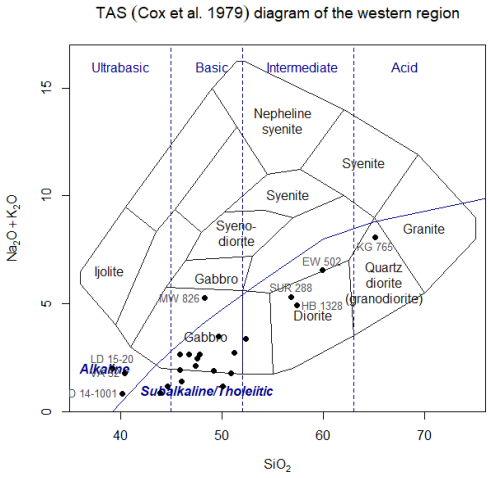

Fig. 5.1: the TAS diagram of the sample bodies of the western region

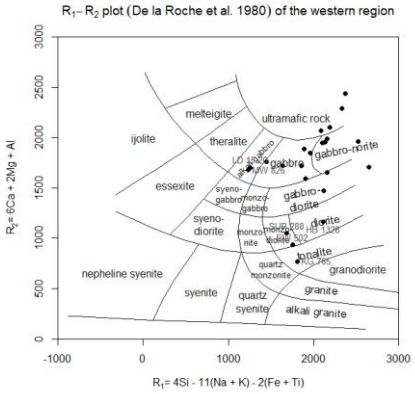

Fig. 5.2: the R1-R2 diagram of the sample bodies of the western region

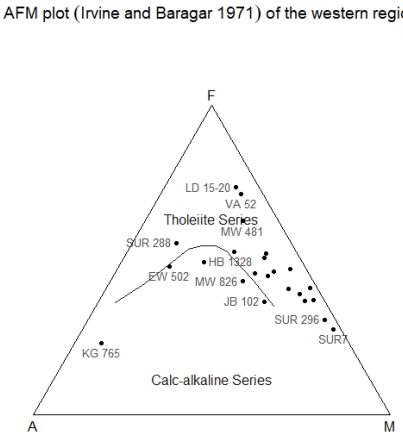

Fig. 5.3: the AFM diagram of the sample bodies of the western region

The Eastern Region

The figures 5.4 to 5.6 shows that the sample rocks of the eastern region has a subalkaline/Tholeiitic basic rocks, mostly ultramafic.

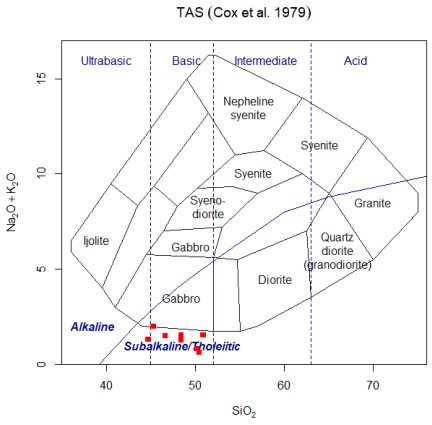

Fig. 5.4: the TAS diagram of the sample bodies of the eastern region

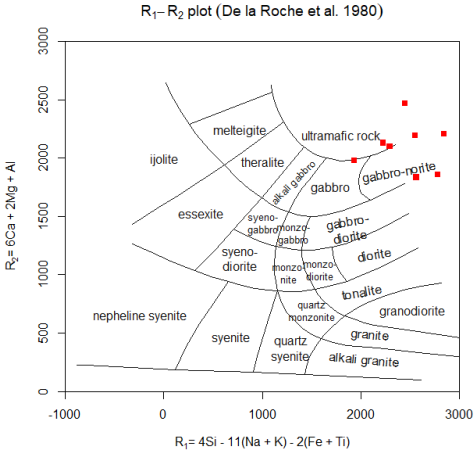

Fig. 5.5: the R1-R2 diagram of the sample bodies of the eastern region

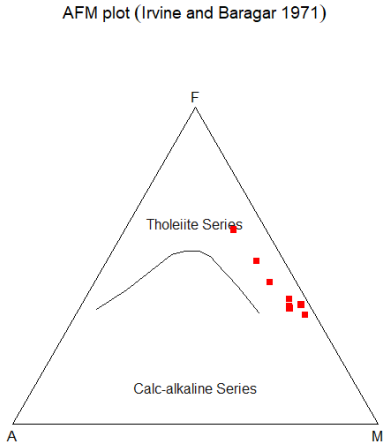

Fig. 5.6: the AFM diagram of the sample bodies of the eastern region

5.2 Geochemistry of the elements according to INAA analyses

The western region

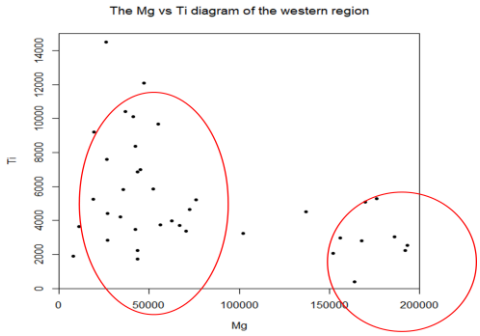

Fig. 5.7: the Mg vs Ti diagram of the western sample bodies

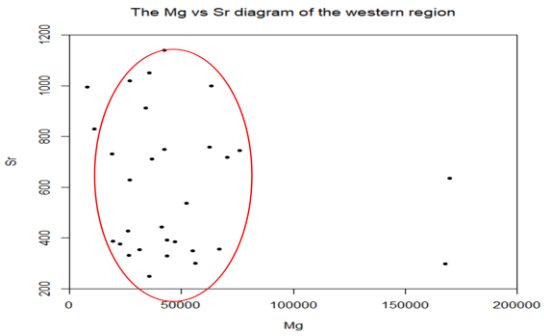

Fig. 5.8: the Mg vs Sr diagram of western sample bodies

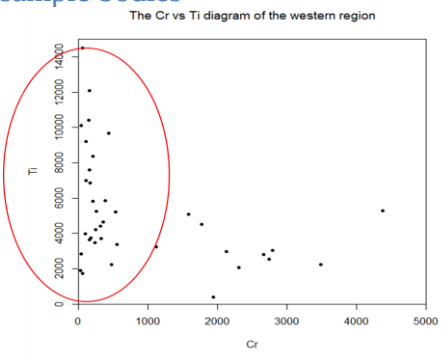

Fig. 5.9: the Cr vs Ti diagram of the western sample bodies

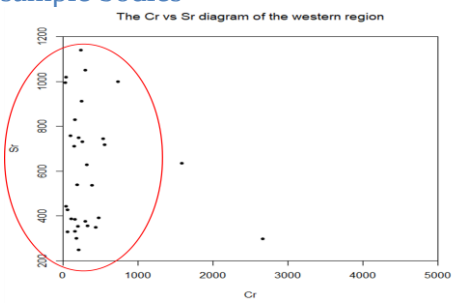

Fig. 5.10: the Cr vs Sr diagram of the western sample bodies

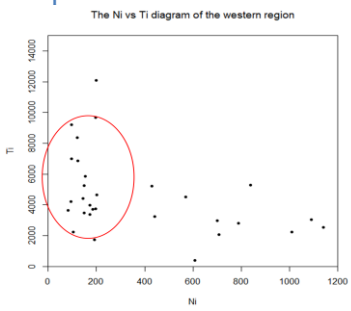

Fig. 5.11: the Ni vs Ti diagram of the western sample bodies

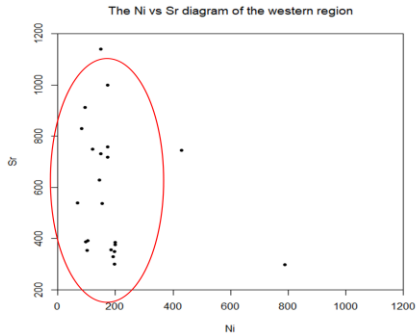

Fig. 5.12.: the Ni vs Sr diagram of the western sample bodies

The Mg vs Ti diagram (fig. 5.7) shows that the western bodies can be divided in samples with high Mg (ultramafic) and low Ti and samples with high Ti and low Mg. Fig 5.8. shows that the samples with a lower Mg grade has high value of Sr. Most of the western bodies has a higher amount of Ti and Sr. The Ni vs Ti diagram, (fig. 5.11) shows that the sample bodies has average amount of Ti versus a low amount of Ni. Fig. 5.12 shows that the samples has a high amount of Sr with low Ni.

The eastern region

The eastern body samples shows a high amount of Mg vs low amount of Ti, but most of the samples has a low amount of Mg and average Ti (fig. 5.13). Also shows the samples that, fig 5.14, they have low amount of Sr vs low Mg. The amount of Ti vs Cr (fig. 5.15) shows that almost at a constant amount of Cr the Ti amount is increasing. At a low Cr the Sr amount is also low and almost constant (fig. 5.16). At an increasing amount of Ni, the amount of Ti is decreasing (fig. 5.17). At an almost constant amount of Ni, the amount of Sr also constant (fig. 5.18).

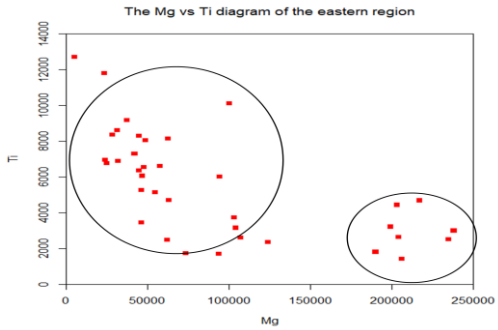

Fig. 5.13: the Mg vs Ti diagram of the eastern sample bodies.

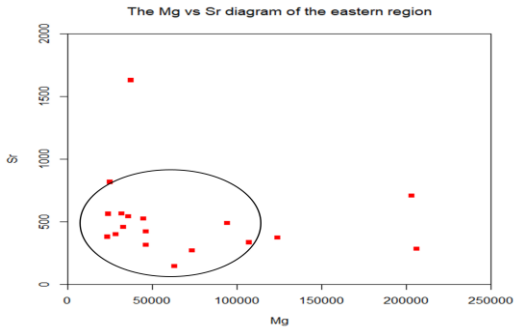

Fig. 5.14: the Mg vs Sr diagram of the eastern sample bodies

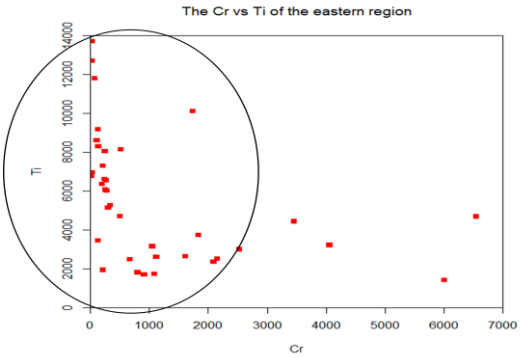

Fig. 5.15: the Cr vs Ti diagram of the eastern sample bodies

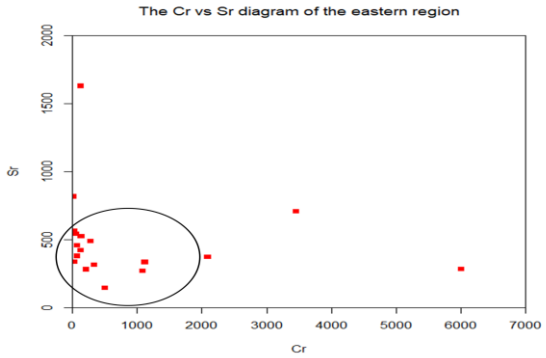

Fig. 5.16: the Cr vs Sr diagram of the eastern sample bodies

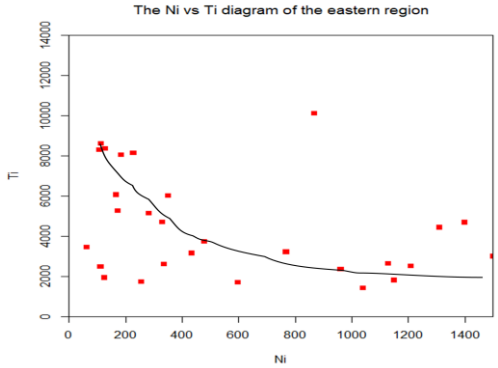

Fig. 5.17: the Ni vs Ti diagram of the eastern bodies

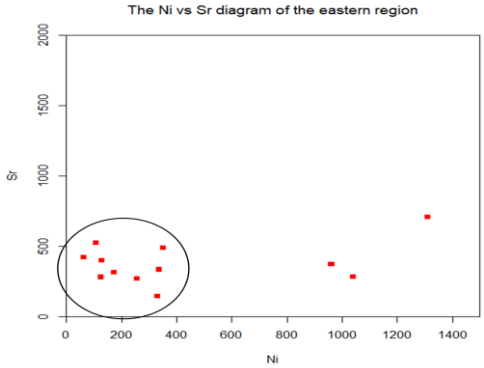

Fig. 5.18: the Ni vs Sr diagram of the eastern sample bodies

5.3 Differentiation trends of the magma

Elements according the XRF data analyses of east and west

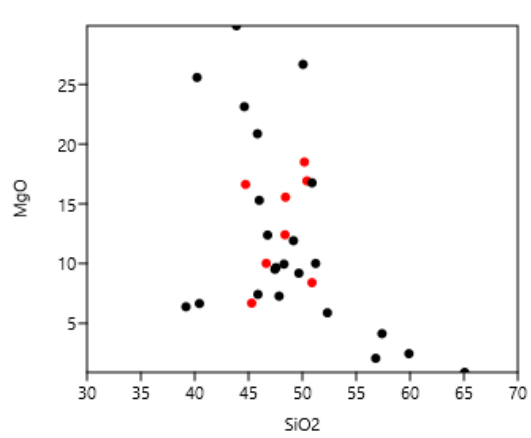

Fig. 5.19: the SiO_2 versus MgO diagram

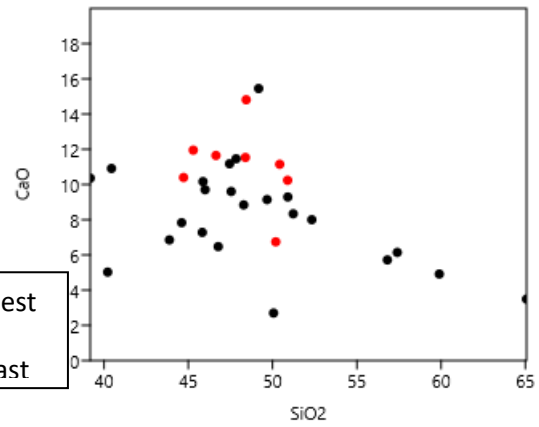

Fig. 5.20: the SiO_2 versus CaO diagram

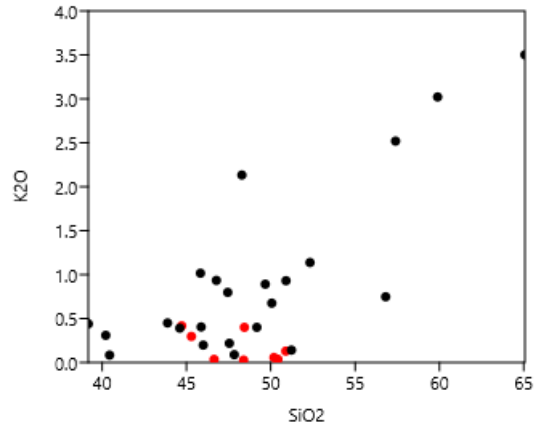

Fig. 5.21: the SiO_2 versus K_2O diagram

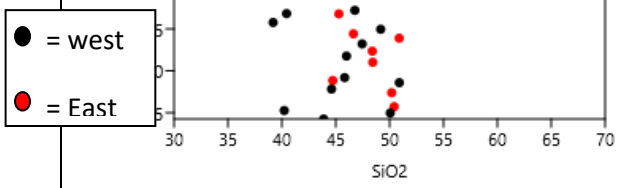

Fig. 5.22: the SiO_2 versus Na_2O diagram

The figures 5.19 – 5.22 shows the diagram of SiO_2 versus the oxides MgO, CaO, K_2O and Na_2O. For both the west and east MgO is increasing at an almost constant value of SiO_2. Looking at the diagram with CaO, for the east the ratio between SiO_2 and CaO is almost the same. But in the west at an increasing SiO_2 the CaO is decreasing. For the K_2O element, in the east is almost zero,

while in the west at an increasing SiO_2 K_2O is also increasing. At last the diagram with the Na_2O, SiO_2 is almost constant while Na_2O is increasing for both east and west.

Elements according to INAA data analyses of east and west

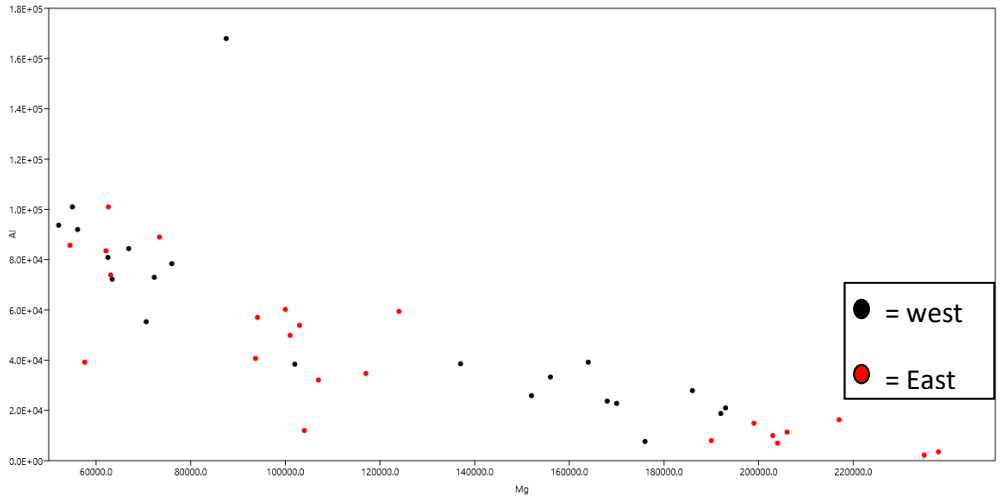

Fig. 5.23: XY graph of Mg vs Al of the elements from the INAA

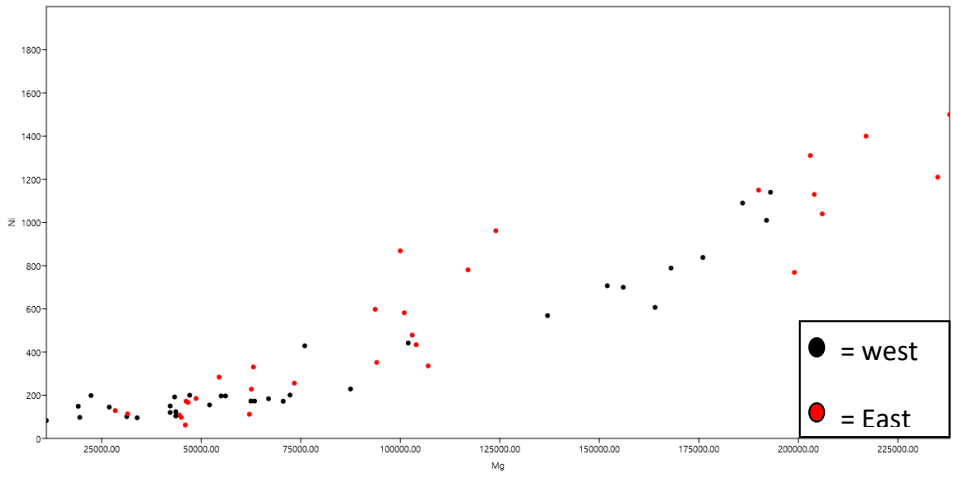

Fig. 5.24: XY graph of Mg vs Ni of the elements from the INAA

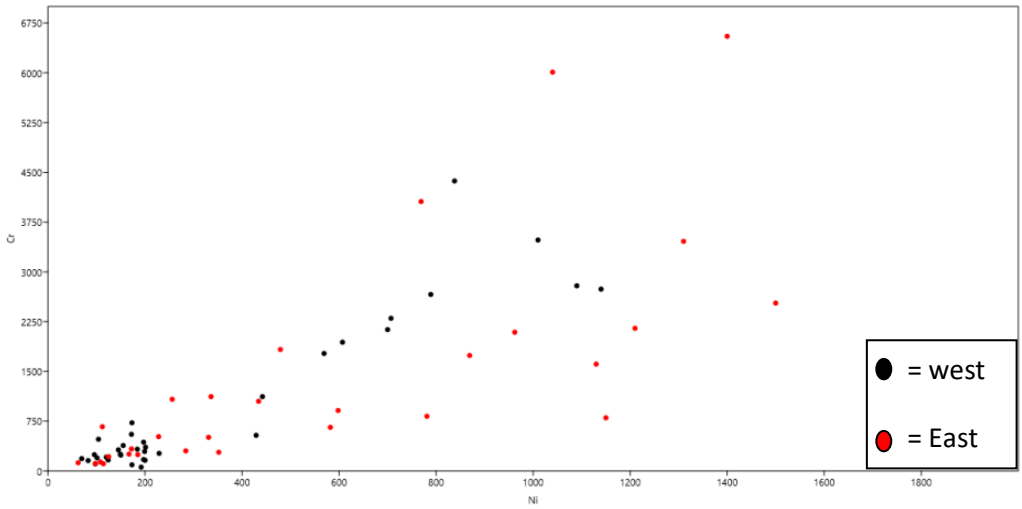

Fig. 5.25: XY graph of Ni vs Cr of the elements from the INAA

The differentiation trend according to fig. 5.10a is that rock samples which are rich in Mg are poor in Al. Figure 5.10b displays a linear trend between Mg and Ni. A rock body sample with high amount of Mg has also an high amount of Ni in it. The positive correlation between Mg and Ni is a characteristic of ultra mafic rocks. Ni and Mg occurs mostly in olivine, which means that the parental magma has an early differentiation. Fig. 5.10c shows that much of the eastern rock samples are richer in Ni, ultramafic.

6. Interpretation

The interpretation is based on the Geostatistics and Geochemistry results.

6.1. Interpretation of the geostatistic analyses

The interpretation of the geostatistics is done according to the analyses described in chapter 4. The skewness of SiO_2, K_2O, P_2O_5, $C2_2O_3$ and Na_2O are positively high. The distribution of the elements are determined by these major elements. The correlation of the XRF elements are also determined by almost these elements. The distribution and correlation of the INAA data set does not show any distinction between east and west. The principal component 3 of the XRF data set shows a distinction between east and west. Component 3 relate with increasing CaO and decreasing Fe_2O_3. There are no clear clustering between the east and west, according the dendrograms of the XRF and INAA data set. The discrimination diagram of the INAA elements gives the elements which can determine the distinction between the two regions. The elements are Mg, La, V, Ti and Cr.

6.2. Interpretation of the geochemistry analyses

The results of the geochemistry analyses (chapter 5) lead to the following interpretations:

The chemical composition and mineralogy of the source region exerts a fundamental control over the chemistry of magmatic rocks. The major and trace element composition of a melt is determined by the type of melting process and the degree of partial melting, although the composition of the melt can be substantially modified en route to the surface. Most magmatic rocks are filtered through a magma chamber prior to their emplacement at or near the surface.

The trace-element discrimination between the gabbroic rocks is also analyzed. The tasks of trace element geochemistry is to discover which geological processes may have this effect and to quantify the extent of a particular process. When the earth's mantle is melted, trace elements display a preference either for the melt phase or the solid (mineral) phase. Trace elements whose preference is the mineral phase are described as compatible, whereas elements whose preference is the melt are described as incompatible. The classification of the lava are done by the appearance of the less mobile elements (Ti, Zr, Y). Also by the concentration of Sr, which indicates a fresh, slightly altered rock. The classification based on Y and Nb diagram, indicates whether the rocks are of alkali or tholeiitic nature. However in the early stages of volcanic the basalts may contain a large proportion of olivine phenocrysts which reduce the absolute amounts of Ti, Zr, Y, Nb and Sr. In this case which can be recognized in altered rocks by abnormally high MgO, Cr or Ni (Pearce & Cann, 1973). The samples of the several locations does not have any concentration of Y and Nb.

The western region

The geochemistry analyses of the major elements indicates a division of the rocks in mostly subalkaline/Tholeiitic basic rocks. The rocks are spreaded from ultramafic, gabbro-norite, gabbro-diorite, diorite, tonalite, gabbro and alkali-grabbro rocks. The trace elements of this region shows higher values of Ti and Sr compared to MgO, Cr and Ni. The less mobile element Ti has a high value in the western region. The traces of Sr shows also a higher value. This means that the rocks of the western region are fresh or slightly altered. The appearance of Mg, Cr and Ni are poor compared to Ti, Zr and Sr, indicates that the rocks were not crystallized in an early stage of the volcanic. So that means also that the elements Sr, Ti and Zr are incompatible.

The eastern region

Looking at this region the geochemistry analyses shows that the rocks are divided in subalkaline/Tholeiitic basic rocks. The rocks are categorised in ultramafic and gabbro-norite rocks. The amount of the less mobile elements of the eastern region are low compared to also a low amount of Mg, Cr and Ni. Thus, the rocks of the eastern region are crystallized in a much later stage of the volcanism, because most of the less mobile elements are compatible according to the geochemistry results.

Magma differentiation trend

According to Nelson (2012) the magma differentiation can be related with SiO_2 and other elements. The expectation is that with increasing of SiO_2 oxides like MgO and CaO should decrease with higher degrees of crystal fractionation because they enter early crystallizing phases, like olivines and pyroxenes. Oxides like H_2O, K_2O and Na_2O should increase with increasing crystal fractionation because they do not enter early crystallizing phases. Looking at the figures 5.19 – 5.22, the trend is almost the same as described by Nelson. MgO and CaO are decreasing with increasing SiO_2. These elements enters an early crystallizing phase. While the oxides K_2O and Na_2O are increasing. There is no great distinction between magma differentiation of the east and west.

7. Conclusion

The research question: What is the origin of the gabbroic-ultramafic bodies in the Guiana Shield of Suriname?

To answer the research question, 2 sub question should be answered:

1. Is there a geochemical distinction between the two generations of gabbroic-ultramafic bodies?
2. If yes, did they originate from different magmas, and what is their geologic significance of the two suites

The geochemistry shows for both regions that the rock are divided in subalkaline/Tholeiitic basic rocks, ultramafic and gabbro-norite. The western region shows rocks which are classified in other divisions also.

The western region is rich in Ti and Sr, while the eastern region is poor in those elements. The rocks of the western region are fresh or slightly altered. They were not crystallized in an early stage of the volcanism. The rocks of the eastern region are crystallized in a much later stage of the volcanism. At some point the crystallization of the rocks shows a distinction between the gabbroic-ultramafic rocks.

If the answer at the sub question is yes, than the conclusion is clear that the bodies are originated from one magma composition, but the crystallization of the bodies is from different stages. The composition of the original melt contains: MgO, SiO_2, Fe_2O_3, CaO, Al_2O_3. The rocks which are crystallized in an early stage of the volcanism are rich in Ti, Zr and Sr, the western region, while the eastern region is poor in these elements. This conclude also that the composition of the melt for all the gabbroic-ultramafic bodies is the same. Looking at the oxides once more, it is again concluded that there is no great distinction between magma differentiation of the eastern and

western region. Still there are differences between the two suites. These differences can be explained as follows:

1. West intruded in granitoid rocks (fig. 1.1), and had incorporated more Si, K and Na. The eastern suite intruded mostly in mafic Paramaka rocks in the greenstone belt, and therefore has been less contaminated with Si, K and Na,, and had higher Mg, Ni and Cr.
2. Possible incomplete data set in the east, because of limited number of samples and possible sampling bias.

The two ages from east and west are from the eastern and western border areas of the country, it is possible that the intervening bodies have intermediate ages, thus reducing the age gap between the two suites, and it is even possible that there was continuous magmatism from 2.18 – 1.98 Ga. If so, it could indicate the presence of a hotspot below a eastward moving Guiana Shield plate. This require additional dating of much more gabbroic bodies.

Answering the research question:

The gabbroic-ultramafic bodies in the Guiana Shield of Suriname resembles the ultramafic complexes in Alaska and the Urals. The Alaskan originates from a depleted mantle source that has undergone metasomatism in a subduction setting. The hornblende rich petrographic character and the occurrence of hornblende in the bodies refers to the hydrous nature of the parental magmas. Furthermore tholeiitic rocks are produced by volcanism in the oceans at mid-ocean-ridges. The magma is from the earth's mantle because of the occurrences of olivine and pyroxene. Both eastern and western bodies present characteristics of Alaskan type intrusions

8. Recommendations

For a secure interpretation and better classification of the gabbro- ultramafic bodies in Suriname, the geostatistical and the geochemical analyses should be repeated with an extended data set of the elements. There should be even number of samples from the two suites.

This research should be repeated with the focus on the elements which describes the most clear distinction between the east and west, the discriminant function elements.

Literature

(http://www.alexstrekeisen.it/english/pluto/troctolite.php - 6th of May 2019)

Bosma, W., Kroonenberg, S.B., Maas, K. and Roever de, E.W.F. (1983): *Igneous and metamorphic complexes of the Guiana Shield in Suriname*- Geologie en Mijnbouw 62: 241-254

Bosma, w., Maas, K., Roever De, E.W.F. (1980): *Petrogenesis of the Gabbroic-ultramafic Bodies in The Northern Guiana Shield (Suriname);* unpublished.

Gibbs, A.k. & Barron, C.N. (1993): *The Geology of the Guiana Shield*. Oxford Monographs on Geology and geophysics no. 22. New York: Oxford.

Gibson,I.L. and Jagam, P. (1980): *Mineral Association of Canada, Toronto, Ontario; short course handbook.* Instrumental neutron activitation analysis of rocks and minerals.

Kroonenberg, S.B., Roever de, E.W.F., Fraga, L.M., Reis, N.J., Faraco, T., Lafon, J. –M., Cordani, U. amd Wong, T.E. (2016): *Paleoproterozoic evolution of the Guiana Shield in Suriname: A revised model.* Netherlands Journal of Geosciences 95-4, 491-522. Doi:10.1017/njg. 2016.10

Linglin Yuan, Xiaohui Zhang, Zhili Yang, Yinghuai Lu, Haihong Chen (2017): *Paleoproterozoic Alaskan-Type ultramfic-mafic intrusions in the Zhongtiao mountain region, North Chine Craton: Petrogenesis and tectonic implications.* Precambrian research 296 (2017) 39-61

Naipal, R., Kroonenberg, S.B. (2016): *Provenance signals in metaturbidites of the Paleoproterozoic greenstone belt of the Guiana Shield in Suriname.* Netherlands Journal of Geosciences 95-4, 467-489. Doi:10.1017/njg.2016.9

Nelson, A.S. (2012): *Magmatic Differentation*. Tulane University.

https://www.tulane.edu/~sanelson/eens212/magmadiff.htm - 7th may 2019

Oosterbaan, W.E., 1975: *The Adampada lateritic nickel deposit.* Geologisch mijnbouwkundig dienst Suriname, Mededeling 23 pp206-213.

Pearce, J.A. and Cann, J., R.(1973).*Tectonic setting of basic volcanic rocks determined using trace elements analyses.* School of environmental Sciences University of East Anglia, Norwich, NOR, England. Earth and planetary Science Letters 19 (1973) 290-300, North Holland Publishing Company.

Pettigrew, N.T. & Hattori, K.,H. (2006): *The Quetico Intrusions of Western Superior Province: Neo-Archean examples of Alaskan/Ural-type mafic-ultramfic intrusions.* Department of earth Sciences, university of Ottawa, Ontario, Canada. Precambrian Research 149 (2006) 21-24

Roever, E.W.F. De, 1975: *Geology of the central part of the Bakhuis mountains, West Suriname.* Geologisch Mijnbouwkundig Dienst Suriname, mededeling 23 pp65-101

Rollinson, H.R. (1993): *Using Geochemical Data: Evaluation, Presentation. Interpretation.* Routledge New York.

Vanderhaeghe, O. Ledru, P., Thieblemont, D. Egal, E. Cocherie, A., Tegyey, M., Milesi, J.(1998): *Contrasting mechanism of crustle growth Geodynamic evolution of the Paleoproterozoic granite-greenstone belts of French Guiana.* Precambrian Research 92 (1998) 165-193

Vletter de, R. (1984): *Contributions to the geology of Suriname.* Geologisch Mijnbouwkundige Dienst Suriname, Mededeling 27 pp13-30

Zhihong Wang, Simon A. Wilde, Jialiang Wan (2010): *Tectonic setting and significance of 2.3-2.1 Ga magmatic events in the Trans-North China Orogen: New constraints from the Yanmenguan mafic-ultramafic intrusion in the Hengshan-Wutai-Fuping area.* Beijing China. Precambrian Research 178 (2010) 27-42.

Attachments

Att. 1: the XRF data set

Loc.	GMD	Petrology	Na2O	MgO	Al2O3	SiO2	MgO	P2O5	K2O	CaO	TiO2	Cr2O3	MnO	Fe2O3
Lu-mo	KG 765	gabbroB	4,57	0,89	17,88	65,07	0,89	0,13	3,50	3,49	0,33	0,00	0,04	3,01
BH-W (4,5)	EW 502	gabbroA	3,54	2,46	14,61	59,89	2,46	0,57	3,02	4,92	1,45	0,01	0,13	9,26
Hbw	HB 1328	gabbroA	2,39	4,14	15,21	57,40	4,14	0,49	2,52	6,14	1,27	0,02	0,14	9,80
Kabo	SUR 288	ultramafisch	4,57	2,07	17,13	56,81	2,07	0,62	0,75	5,72	1,79	0,00	0,26	10,22
Mrt	SUR 6	gabbroA	2,23	5,88	16,44	52,32	5,88	0,35	1,14	8,00	1,06	0,03	0,17	11,37
Ada	AH 207	GabbroB	2,57	10,01	13,46	51,22	10,01	0,15	0,14	8,34	0,74	0,07	0,17	11,47
Mask	SUR 300	gabbroB	0,86	16,76	6,95	50,90	16,76	0,11	0,93	9,29	0,52	0,15	0,21	13,13
Mask	SUR 296	ultramafisch	0,50	26,69	4,59	50,06	26,69	0,09	0,68	2,70	0,30	0,36	0,23	13,75
BH-W (4,5)	EW 500	gabbroA	2,59	9,20	14,65	49,67	9,20	0,47	0,89	9,14	1,09	0,06	0,17	11,83
Ston	LD 14-901	gabbroB	1,50	11,92	9,84	49,17	11,92	0,12	0,40	15,45	0,50	0,08	0,17	10,55
Hbw	JB 102	gabbroA	2,57	7,28	24,52	47,84	7,28	0,06	0,09	11,46	0,07	0,01	0,08	6,37
Hbw	FO 810	GabbroA	2,22	9,67	17,44	47,54	9,67	0,06	0,22	9,61	0,66	0,02	0,19	13,84
Mask	SUR 298	GabbroB	1,32	9,52	14,67	47,45	9,52	0,10	0,80	11,18	0,68	0,01	0,16	14,00
Ston	LD 14-30	gabbroB	1,72	12,39	14,71	46,77	12,39	0,32	0,94	6,47	0,80	0,07	0,16	14,38
BH-W (6)	MW 481	gabbroA	2,26	7,42	13,36	45,87	7,42	0,12	0,41	10,17	2,08	0,02	0,19	18,73
Kabo	SUR 286	ultramafisch	0,92	20,88	6,97	45,83	20,88	0,18	1,02	7,28	0,63	0,23	0,22	14,74
Kabo	SUR 285	ultramafisch	0,78	23,14	6,10	44,61	23,14	0,11	0,39	7,83	0,50	0,25	0,23	15,86
Ada	SUR7	ultramafisch	0,42	29,92	3,64	43,88	29,92	0,07	0,45	6,86	0,26	0,41	0,21	12,99
Ston	LD 14-1001	ultramafisch	0,53	25,59	4,04	40,21	25,59	0,28	0,31	5,03	0,65	0,22	0,30	20,32
Ston	LD 15-20	Gabbro	1,58	6,38	14,16	39,18	6,38	0,24	0,44	10,36	1,78	0,02	0,21	25,79
Awa	ACK 26-100	GabbroB	2,79	7,08	17,31	52,39	7,08	0,09	0,65	10,27	0,60	0,02	0,14	8,32
DGj	CS 579	GabbroB	1,39	8,41	16,43	50,89	8,41	0,03	0,13	10,24	0,39	0,03	0,22	11,66
Piq	ES 2	gabbroB	0,57	16,92	8,89	50,42	16,92	0,02	0,04	11,15	0,28	0,13	0,20	11,74
Piq	D 1065	GabbroB	0,74	18,51	11,01	50,19	18,51	0,02	0,06	6,75	0,26	0,29	0,16	11,25
GR	EP 2589	GabbroB	1,10	15,56	5,65	48,43	15,56	0,05	0,40	14,81	0,42	0,16	0,20	11,25

DGj	CS 73	GabbroB	1,24	12,41	17,46	48,39	12,41	0,01	0,03	11,54	0,20	0,15	0,16	8,73
DGj	MC 182	GabbroB	1,44	10,02	18,23	46,64	10,02	0,02	0,04	11,65	1,27	0,07	0,16	10,36
GR	EP 2594	GabbroB	1,68	6,69	18,87	45,29	6,69	0,08	0,30	11,95	1,32	0,02	0,14	15,25
Awa	ACK 27-95	GabbroB	0,88	16,63	9,75	44,72	16,63	0,15	0,42	10,40	0,45	0,25	0,18	13,00

Att. 2: the INAA data set

	Location	GMD	Petrology	Na	Mg	Al	Ca	Sc	Ti	V	Cr	Mn	Fe	Co	Ni	Sr	La	Ce	Eu	Tb	Yb	Lu	Hf
YE028	Ada	LA 202-33	ultra-maf	4250	186000	27900	74500	28,9	3050	85,3	2790	1730	89100	103	1090		3,56		0,688	0,206	0,631	0,0915	0,693
YE022	Ada	VA 52	gabbroA	11400	41300	75900	66800	49,7	10100	1260	40	1300	154000	112		443	1,55		0,585		0,677		0,597
YC006	Ada	AH 920	gabbro	8050	66900	84400	85100	45,3	3700	295	328	1670	75500	65,7	184	355	1,58		0,516		1,42	0,21	0,704
YA004	Ada	SUR 7	ultra-maf	3740	193000	21000	30200	23,9	2520	87,5	2740	1620	74800	95,6	1140		3,92	18,7	0,615		0,687	0,111	0,622
MB004	Ada	AH 920	gabbro	7440	22300	20700	71700	38,6		60,1	294	1780	86800	75	199	375	1,62	5,56	0,319	0,189	0,642	0,0802	
MA004	Ada	AH 920	gabbro	6950	72300	73000	91700	5,59	4640	498	358	1610	84500	77,4	201		1,7	4,8	0,428		0,862	0,116	0,677
YE026	Awa	ACK 27-915	gabbroB	6390	103000	53900	75100	35,5	3720	153	1830	1430	85200	83,7	479		6,88	16,7	0,775		0,844		0,785
YE024	Awa	ACK 26-100	gabbroB	18000	46000	100000	54000	28,1	3450	180	124	1190	52500	34,2	62,1	419	8,02	17,7	0,782		0,631	0,268	0,959
MB002	Awa	ACK 26/100	gabbroB	23700	35800	93200	71100	28,2			63,7	405	43900	33,2		542	8,18	20,7	0,64	0,512	0,868	0,0784	0,971
MA002	Awa	ACK 26/100	gabbroB	20700	32800	87400	79300	27,8		79,8	71,2	1070	45900	36,2		456	8,97	14,9	0,843	0,263	0,659		0,929
YF014	Bem	LD 3-121	ultra-maf	2170	104000	12000	148000	75,4	3150	167	1050	1400	54300	66,2	434		1,5	5,89	0,778	0,85	0,806		0,688
YF01	Bem	LD 3-66	ultra-maf	619	1900	7990	4050	18	180	51,80	15	1090	17	11		1,3		0,2					

2					00		0		0	4	1	40	00	4	50		9		09				
YF010	Bem	LD 3-44	ultra-maf	118	235000	2190	14600	3,55	2500	16,8	2150	1900	114000	209	1210		0,852						
YF008	Bem	LD 2-46	ultra-maf	765	204000	7000	31700	19,8	2630	69,1	1610	1650	121000	175	1130		1,17				0,393		
YF006	Bem	LD 2-44	ultra-maf	410	238000	3520		6,37	2990	56,7	2530	2030	129000	204	1500		0,747						
YF004	Bem	LD 2-31	ultra-maf	1310	203000	10000		8,99	4430	103	3460	2070	126000	184	1310	705	2,95				0,269		0,38
MB018	BHW	MW 481	gabbroA	21000	19100	97900	43500	13,3	5240	121	253	1110	56800	40,2	149	732		19,7	0,924		0,689	0,0968	1,65
MA018	BH-W	MW 481	gabbroA	20800	26900	91700	79200	33,1	4420	145	318	1230	60800	50,4	145	628	18,7	47,8	1,17	1,04	2,27	0,344	1,21
YD010	BHW 4+5	EW 502	gabbroA	22400	19500	89000		17,4	9190	186	107	1110	58000	12	97,5	386	44,1	98,7	1,92	0,488	2,57	0,373	6,32
YD008	BHW 4+5	EW 500	dolerite gabbro	17700	55000	101000	52800	30,1	9680	237	434	1620	74900	50,9	197	349	23,3	48,1	1,83	0,563	2,08	0,481	3,16
YE010	BHW 6	MW 481	gabbroA	16700	47100	73800	102000	40,5	12100	563	161	1510	127000	83	200	384	9,74	19,6	1,3	0,365	1,63	0,163	1,21
YE008	BHW 6	MW 480	gabbro	18100	52100	93700		22,2	5840	170	384	1320	67800	45,8	155	536	17,8	37,4	1,31	0,565	1,52		1,22
YD022	BHW 6	JU 337	gabbro	18400	26200	78700	63500	32,7	14500	385	56,4	1740	103000	42,4		427	59,6	134	2,97	1,62	4,22	0,596	7,43
MB014	CNI	KG 768	diorGabb	27800	42200	84000	52800	19,1	8380	171	207	1420	54200	33,2	120	748	32,3	88	1,64	1,55	3,39	0,554	6,45
MA014	CNI	KG 768	diorGabb	28800	11100	56000	45200	14,4	3640	70,9	156	525	36300	21,5	82,7	830	26,3	69,3	1,6	0,942	2,43	0,306	4,49
YC014	CNIN	CS 910	ultra-maf	14400	43600	81100	88100	42,3	6850	332	166	1930	97200	61,8	124		7,03		1,19	0,537	2,81		1,39
MB006	CNIZ	CS 680		8470	87500	168000	73800	33,5		399	265	2910	78300	88,2	229		1,58		0,266	0,249	0,616	0,0747	0,52
MA006	CNIZ	CS 680		18200	63400	72200	83000	3,83		184	726	1480	68700	49,2	173	1000	37,4	92,6	1,54	1,13	1,58		2,76
YE02	DGj	ST 116	gabbro	270	4620	8800	5330	23	526	195	33	13	6340	35,	17	31	6,7	15	0,8	0,7	1,8	0,46	1,6

0				00	0	0	0	,9	0		2	10	0	5	2	5	2	,9	16	11	6	6	6
YE018	DGj	ST 112	gabbro	24200	23300	109000	87300	27,2	11800	206	69,8	2060	82000	35,3		378	16,1	37	1,7	0,727	2,64	0,497	4,889
YE016	DGj	SE 82	gabbro	8860	94100	57000	62700	47	6010	361	282	2140	113000	101	352	488	2,97		0,905	1,09	0,972	0,331	0,888
YE006	DGj	MC 183	ultra-maf	5210	100000	60200	68800	28,4	10100	234	1740	1570	90900	87	869		14,9	18,4	1,56	0,791	1,9	0,217	2,3
YE004	DGj	MC 182	gabbroB	11100	62600	101000	68500	27,6	8130	175	518	1320	67300	58,2	228		0,561		0,5		0,646	0,0853	0,412
YC012	DGj	CS 73	gabbroB	9240	73400	89000	106000	27,6	1720	166	1080	1220	57800	60	256	270	0,638		0,439			0,126	
YC010	DGj	CS 59	ultra-maf	3800	57600	39200	117000	55,7	6600	423	243	1830	90200	62			1,82	9,08	0,751	0,317	1,63	0,286	0,862
YC008	DGj	CS 57A	gabbro				71100	35,2	1930	220	215	1700	77800	56,7	125	280	5,66		0,919	0,25	0,655	0,125	0,524
YC004	DGj	AN 207	gabbro	18600	63100	73900	54900	25,4	4700	177	507	1340	75200	50,6	331	143	7,07	15,9	0,297	0,42		0,17	1,32
YC002	DGj	AN 191	gabbro	11800	62100	83500	64200	34,4	2480	197	667	1500	68800	54,8	112		0,942		0,688		0,79		
MB016	DGj	LC 5/30,15	metagabbro	21500		133000		32,3	13700	177	29,7	2950	95300	36,2		337	14,6	32,4	1,81	1,08	3,74	0,549	8,17
MA016	DGj	LC 5/30,15	metagabbro	20800	5000	104000	62200	31	12700	177	33,1	2780	96900	35,6			16,2	32,9	1,86	0,761	3,39	0,467	8,73
YF002	Emm	LC 18-9	ultra-maf	638	176000	7650	191000	18,8	5280	77,6	4370	1370	63400	95	838		0,432		0,237				
YC028	GR	EP 2594	gabbro	12300	44500	112000	73900	31,8	8290	551	135	1180	97500	6404	108	524	4,42		0,609		1,02		
YC026	GR	EP 2589	gabbroB	7910	107000	32100	102000	49,9	2600	188	1120	1760	73200	66	336	333	10,5	29	1,08	0,866	1,05	0,154	1,37
MB008	GR	EP 2594	gabbroB	11400	24100	94300	94100	30,8	6940	551	28,6	1140	96800	66		561	2,98	6,37	0,335		0,348		
MA008	GR	EP 2594	gabbroB	12100	28400	113000	82600	2,54	8360	573		896	80100	64,1	129	399	3,63	10,4	0,499		0,534	0,0407	0,703
YD0	Hbw	JB 104	gabbro	223	4360	1140	6280	22	222	82,	47	11	6240	43	10	39	2,5		0,4		0,7		0,4

18				00	0	00	0	,9	0	9	8	30	0		4	1	8		57		14		24
YD0 16	Hbw	JB 102	gabbroA	180 00	4330 0	1320 00	7830 0	4, 46	172 0	40, 7	57	61 8	4020 0	46, 6	19 2	32 8	2,0 3	3, 88	0,4 26	0,0 76	0,3 09		0,4 24
YD0 14	Hbw	HB 1328	gabbroA	156 00	2630 0	8530 0		23 ,1	761 0	188	15 3	11 40	5970 0	28, 9		33 0	57, 6	12 5	2,2	0,7 11	3,6 3	0,55 1	6,7 7
YD0 12	Hbw	FO 810	gabbro	163 00	5610 0	9200 0	6000 0	25 ,4	374 0	167	17 2	14 20	8840 0	68, 1	19 7	29 9	3,1 5	8, 31	0,7 23	0,1 48	1,3 2	0,22 7	1,1 5
MB0 12	Hbw	JB 104	gabbro	235 00	3130 0	1180 00	6940 0	16 ,5			19 7	82 4	3970 0	35, 9	10 1	35 4	2,4 2	6, 36			0,4 66		0,4 28
MA0 12	Hbw	JB 104	gabbro	254 00		1250 00	8090 0	1, 39			18 6	68 3	3600 0	32, 2	69, 4	53 9	2,2 6	5, 6	0,4 08	0,4 58	0,4 58		0,3 41
YB0 02	Kabo	SUR 291	ultra-maf	689 0	1560 00	3330 0	4730 0	20 ,9	297 0	142	21 30	17 30	1070 00	12 4	70 0		5,1 4	22	0,4 61	0,1 56	0,6 55	0,09 18	0,7
YA0 28	Kabo	SUR 286	ultra-maf	735 0	1370 00	3860 0	7590 0	29 ,8	450 0	161	17 70	16 00	1020 00	11 4	56 9		7,8 5	26 ,1	0,7 67		1,5 2		1,1 2
YA0 26	Kabo	SUR 285	ultra-maf	668 0	1640 00	3920 0	4970 0	31 ,5	400	192	19 40	19 90	1060 00	12 2	60 7		4,6 1	17 ,4	0,5 76		0,5 81		0,8 98
YE00 2	LuMo	KG 768	gabbro	292 00	3390 0	9820 0		19 ,6	420 0	145	24 5	11 70	4630 0	26, 2	95, 6	91 2	26, 9	62 ,1	2,2 8	0,8 18	2,9 7	0,43 4	5,1 2
YD0 30	LuMo	KG 765	diorite-gabbro	314 00	7760	9800 0		2, 61	191 0	35	24, 1	34 3	1980 0	7,0 7		99 4	23, 6	43 ,4	1,9 9	0,3 08	1,2 8		2,4 3
YD0 28	LuMo	KG 760	diorite-gabbro	235 00	2670 0	1260 00	7280 0	18 ,9	285 0	152	33, 4	93 1	4260 0	31		10 20	13, 2	26 ,6	0,9 45	0,2 13	1,3 6		1,7 1
YB0 14	Mask	SUR 301	ultra-maf	296 0	1920 00	1880 0		10 ,1	222 0	63, 5	34 80	15 60	9880 0	15 4	10 10		374	15 ,5	0,3 93	0,5	0,5 82	0,05 97	0,7 44
YB0 12	Mask	SUR 300	gabbroB	683 0	1020 00	3840 0	7850 0	47 ,8	325 0	147	11 20	15 90	8560 0	69, 1	44 2		10, 1	29 ,9	0,8 85		1,1 5	0,15 7	1,5
YB0 10	Mask	SUR 298	gabbroB	103 00	6250 0	8090 0	7140 0	37 ,6	397 0	267	92, 6	13 40	9230 0	56, 7	17 3	75 7	9,9 1	30 ,8	0,8 58	0,6 66	1,0 7	0,19 8	1,5 7
YB0 08	Mask	SUR 296	ultra-maf	427 0	1680 00	2370 0		24 ,4	280 0	82, 1	26 60	17 80	8900 0	11 1	78 9	29 8	7,2	25 ,4	0,9 18		0,5 91	0,06 91	1,1 1
YB0 06	Mask	SUR 295	ultra-maf	433 0	1520 00	2590 0		27	207 0	78, 4	23 00	17 10	8290 0	96, 5	70 7		6,8 6	22 ,1	0,4 61				0,8 47
YA0	Mrt	SUR 6	gabbroA	154	3560	9030	5500	24	582	189	20	13	6810	34,		24	32,	90	169	0,7	2,5	0,49	3,8

02				00	0	0	0	,9	0		7	80	0	6		8	2	,7		74	3	3	5
MB022	Oel	SM 19		9610	24700	90500	91800	39,3	6760	56000	18,4	1290	106000	63,5		816	2,17		0,301		0,268	0,0368	
MA022	Oel	SM 19		8420	31900	80400	92200	42,4	6890	588	19,8	1410	111000	66,3		563	1,95	5,14	0,43		0,317		
YD020	Para	JN 243	meta dolerite	24900	47700	75700	69900	47,3	6540	311	262	1710	94600	56,4			2,84	6,8		0,792	2,38	0,392	1,89
YD006	Para	ES 680	meta dolerite	28800	46700	81000	61500	45,2	6060	243	254	1460	78200	52,3	167		13	18,2	2,74	1,5	5,38	0,704	1,64
YC022	Para	EG 508	metagabbro	13700	42000	70300	57200	44,1	7300	301	216	1790	101000	60,8			4,39	9,34	1,1	0,958	2,35	0,395	1,72
YC020	Para	EG 484	metagabbro	11500	54500	85700	79500	29,1	5140	130	303	1430	82000	65,3	284		3,82	8,04	0,726	0,858	1,58	0,206	1,27
YB024	Para	SUR 349	metabasalt	15300	48700	85300	88500	38,3	8040	318	246	1680	91600	54,2	185		4,78	15,3	0,807	0,404	2,1	0,423	1,98
YB022	Para	SUR 348	metabasalt	13900	44800	78200	70900	39,1	6360	287	200	1520	85700	52			3,72		0,796	0,679	2,12	0,365	1,7
YB020	Para	SUR 346	metabasalt	15000	31500	75200	91800	36,4	8620	376	109	1840	101000	48,9	114		5,89	17,9	0,944		2,27	0,35	2,53
YB004	Para	SUR 294	metabasalt	17900	45000	74700	78300	37,8	7010	294	110	1690	94900	53,7	97,4		4,82		1,18	0,49	2,46	0,332	2,12
YA024	Para	SUR 280	metabasalt	8980	37300	79300	47700	38,2	9160	351	125	1570	94400	46,8		1630	6,77	19,1	1,35	0,89	2,93		2,35
YD002	Piq	ES 29	ultra-maf	839	217000	16300	17400	18,4	4680	93,1	6550	1860	82300	97,5	1400		27,3				0,332		
YC030	Piq	ES 2	gabbroB	5000	93700	40700	67100	43,9	1700	96,6	911	1420	78000	81,6	598		1,47		0,493		0,653		
YC018	Piq	D 1065	gabbroB	6280	124000	59400	58500	22,2	2350	97,9	2090	1280	75200	69,9	962	372	1,04		0,379		0,607	0,0908	
YC016	Piq	D 1060	ultra-maf	816	206000	11400		18,8	1420	89,5	6010	1860	82200	92,2	1040	283	2,3		0,235		0,293		
MB010	Piq	ES 2	gabbroB	5270	101000	49900	101000	45,4		127	658	1480	59600	71,2	582		1,18	5,29	0,27		0,412		
MA0	Piq	ES 2	gabbroB	321	1170	3470	8510	4,		131	82	16	7410	92,	78		1,0		0,2		0,4	0,05	0,4

10				0	00	0	0	8			4	50	0	6	1		1		76		44	91	97
YE030	Sara-Up	LB 159-50	ultra-maf	890	199000	14900		21,7	3210	67,9	4060	1350	57400	641	769		2,61	8,47					
MB020	Sip	OB 3649		21400	42200	94800	68900	25,8	3480	144	239	1130	57100	37,8	150	1140	10,2	22,8	0,846	0,388	0,801	0,062	1,01
MA020	Sip	OB 3649		21000	35400	88900	82100	23,5		172	292	1260	70500	46		1050	19,1	47,3	1,08	0,516	0,9		1,04
YF022	Ston	LD 15-20	gabbro	10600	36700	76800	89700	39,2	10400	918	144	1610	166000	79,3		711	12,8	31,1		0,446	1		1,27
YF020	Ston	LD 14-1001	ultra-maf	4270	170000	22800	49700	20,4	5070	151	1580	2370	130000	136		634	15,9	37,2	0,956	0,274	0,78	0,594	0,987
YF018	Ston	LD 14-901	gabbroB	10300	70600	55300	112000	54,8	3370	165	552	1370	66500	47,7	172	717	12,4	30,5	1,29		0,991		1,32
YF016	Ston	LD 14-30	gabbroB	12000	76000	78400	46100	14	5230	153	537	1220	93300	82	429	744	22,1	48	1,2	0,344	0,805		1,47